Aalto University
School of Electrical
Engineering

Aapeli Takala

Volumetric thermometry with proton resonance

Thesis submitted for examination for the degree of Master of Science in Technology.

Espoo July 14th, 2015
Thesis supervisor: Prof. Raimo Sepponen
Thesis advisor: D.Sc (Tech.) Toni Auranen

Aalto University
School of Electrical
Engineering

Aalto University, P.O. BOX 11000, 00076
AALTO
www.aalto.fi

Abstract of master's thesis

Author Aapeli Takala		
Title of thesis Volumetric thermometry with proton resonance		
Degree programme Bioinformation technology		
Major Bioengineering		**Code** F3013
Thesis supervisor Raimo Sepponen		
Thesis advisor Toni Auranen		
Date 14.07.2015	**Number of pages** 71	**Language** English

Abstract

Proton resonance frequency (PRF), by which it precesses in the magnetic field, alters due to change in temperature, which can be detected with magnetic resonance imaging (MRI). MRI scanner uses protons' nuclear magnetic resonance phenomenon. The target is first excited with a radio frequency pulse, then it's relaxation to initial stage is observed. Parts with different temperatures can be mapped according to the characteristics of the signal they emit during relaxation. PRF thermometry is recognized as the best method to study in vivo temperature distribution with MRI scanner. PRF thermometry is favored due to a good large scale linearity and tissue independence.

When tissue containing water is heated, the hydrogen bonds between water molecules are soften as a result of increased Brownian motion. When hydrogen bonds are weaker, the magnetic shielding from electron cloud around proton is stronger. Now that the magnetic shielding is stronger, the local magnetic field of that proton is weakened. Lower magnetic field leads to lower proton nuclear magnetic resonance. Change in nuclear magnetic resonance can be detected with phase difference mapping as a phase shift in phase images with MRI scanner.

Noninvasiveness is universally justified in clinical medicine. Diseases and tumors in living tissues can be noninvasively treated with hyper- or hypothermia. Abnormal situations can be detected by observing the temperature changes in the body. MRI scanner can be used to examine tissue temperatures during temperature treatments. Temperature mapping can also be used to monitor unwanted tissue heating related to MRI examinations. The purpose of this thesis is to produce volumetric thermometry data with proton resonance, and to optimize the imaging parameters in order to achieve the best signal-to-noise ratio for magnetic resonance thermometry.

Keywords MR thermometry, PRF thermometry, phase difference mapping

Aalto-yliopisto
Sähkötekniikan
korkeakoulu

Aalto-yliopisto, PL 11000, 00076
AALTO
www.aalto.fi

Diplomityön tiivistelmä

Tekijä Aapeli Takala

Työn nimi Kolmiulotteinen lämpötilamittaus protoniresonanssin avulla

Koulutusohjelma Bioinformaatioteknologia

Pääaine Biologinen tekniikka **Koodi** F3013

Työn valvoja Raimo Sepponen

Työn ohjaaja Toni Auranen

Päivämäärä 14.07.2015 **Sivumäärä** 71 **Kieli** Englanti

Tiivistelmä

Protonin resonanssitaajuus (PRF), jolla se prekessoi magneettikentässä, muuttuu lämpötilan muutoksen johdosta, joka voidaan nähdä magneettikuvauslaitteen avulla. Magneettikuvauslaite käyttää hyväkseen protonien ydinmagneettista ilmiötä. Kohdetta viritetään ensin radiotaajuuspulssilla, jonka jälkeen seurataan sen palautumista alkutilaan. Eri lämpöiset alueet kohteessa voidaan kartoittaa niiden lähettämän eri taajuisen signaalin avulla palautumisen aikana. PRF muutos on tunnustettu parhaaksi menetelmäksi seurattaessa elävien kudosten sisäisiä lämpötilaeroja magneettikuvauslaitteen avulla. Etuna PRF menetelmässä toisiin magneettikuvauksen avulla tehtäviin lämpömittausmenetelmiin on sen hyvä lineaarisuus laajalla mittausalueella, ja riippumattomuus kudostyypistä.

Kun vettä sisältävä kudos lämpenee, siinä olevien vesimolekyylien väliset vetysidokset heikkenevät lisääntyvän lämpöliikkeen vuoksi. Kun vetysidokset heikkenevät, kasvaa veden protonien ympärillä olevien elektronipilvien magneettinen suojaus. Kun magneettinen suojaus kasvaa, kokee protoni magneettikuvauslaitteen magneettikentän paikallisesti heikompana. Kun paikallisesti koettu magneettikenttä on heikompi, on myös protonin resonanssitaajuus pienempi. Tämä havaitaan magneettikuvauslaitteen vaihekuvissa vaihe-erona. Vaihemuutoskartan avulla voidaan kartoittaa kohteen lämpötilaeroja.

Minimaalinen kajoamattomuus on yleisesti perusteltua lääketieteellisissä hoidoissa. Kehon lämpötilamuutosten avulla saadaan tietoa kehon anomaalisista tiloista. Elävissä kudoksissa olevia tauteja ja kasvaimia voidaan hoitaa kajoamattomasti lämpö- ja kylmäterapialla. Magneettikuvauslaitteella voidaan seurata kudosten lämpötilaa hoitojen aikana, sekä kartoittaa kehon poikkeavia lämpötilaeroja. Vaihekartoituksen avulla voidaan seurata myös magneettikuvaukseen liittyvää kudosten lämpenemistä. Tämän työn tavoitteena on muodostaa lämpötilatietoa kuvaava tilavuuskartta protonin resonanssitaajuuteen perustuvalla menetelmällä, ja optimoida kuvausparametrejä parhaan signaalikohinasuhteen saavuttamiseksi lämpötilamittauksen osalta.

Avainsanat Magneettikuvaus lämpötilamittaus, protoniresonanssitaajuus, vaihemuutoskartta

Preface

This thesis was done at Aalto University Advanced Magnetic Imaging (AMI) Centre, which is part of Aalto NeuroImaging research infrastructure. Aalto NeuroImaging is part of Department of Neuroscience and Biomedical Engineering (NBE) in Aalto School of Science. This thesis acts as an introduction to the magnetic resonance thermometry, and answers the questions how and why to produce volumetric thermal maps with regular MRI scanner.

My introduction to magnetic resonance imaging started with Picker Nordstar Merit 0,1T MRI Scanner at School of Electrical Engineering, which made my mind spin. Comprehensive studies of magnetic resonance imaging studies somehow draw me towards AMI Centre, and the reason appeared to be the Siemens Skyra 3T MRI scanner.

I would like to thank Raimo the supervisor of the thesis for exciting topic, and Toni the advisor for technical support. Also the staff of AMI centre deserves acknowledgement for an open and pleasant working atmosphere. Again thanks goes of course to my family, friends, and love Marika.

Espoo 14.7.2015

Aapeli Takala

Contents

Symbols

α	PRF temperature coefficient
B_0	static magnetic field
δ	duration of gradient pulse
E_a	activation energy
$E_{½}$	energy state of the spin aligned parallel to the static magnetic field
$E_{-½}$	energy state of the spin anti-aligned parallel to the static magnetic field
ϕ	wrapped phase
θ	unwrapped phase
θ_E	Ernst angle
G	gradient strenght
G_F	frequency encoded gradient field
γ	gyromagnetic ratio
h	Planck's constant
$\hbar$	reduced Planck's constant
J	angular momentum
k_B	Bolzmann's constant
M_0	net magnetization
M_{xy}	transversal part of the net magnetization
M_z	vertical part of the net magnetization
m	the temperature dependence of the T_1 relaxation time
N_a	number of proton spins aligned antiparallel
N_p	number of proton spins aligned parallel
S	image signal strength
SD	standard deviation
s	spin number
σ	standard deviation
T_1	longitudinal / spin-lattice relaxation time
T_2	transversal / spin-spin relaxation time
T_2^*	transversal relaxation time with inhomogeneities
T_m	phase transition temperature
μ_0	permeability of vacuum
χ_0	susceptibility
ω_0	Larmor frequency

Abbreviations

CSI	chemical shift imaging
DSV	diameter of spherical volume
FOV	field of view
FA	flip angle
fMRI	functional magnetic resonance imaging
GRAPPA	Generalized autocalibrating partially parallel acquisition
GRE	gradient echo
MASTER	multiple adjacent slice thermometry with excitation refocusing
MR	magnetic resonance
MRI	magnetic resonance imaging
NMR	nuclear magnetic resonance
PRELUDE	Phase Region Expanding Labelled for Unwrapping Discrete Estimates
PRF	proton resonance frequency
PVC	poly vinyl carbonate
ppm	parts per million
RF	radio frequency
ROI	region of interest
SAR	specific absorption rate
SE	spin echo
SNR	signal-to-noise ratio
TE	time to echo / echo time
TI	time to inverse / inverse time
TR	time to repeat / repetition time

1 Introduction

In medicine, the treatment of a patient needs to be done in the most ethical way. The best interest of the patient should always be the main concern. One of the basic medicine guideline, originating from the Hippocratic Oath, is “to abstain from doing harm”. This promise is nowadays implemented in the seek of the least harmful examination methods such as noninvasive imaging modalities.

Magnetic resonance imaging (MRI) has become one of the most important medical imaging modalities within the past couple of decades. Most MRI examinations can be done without any harm, noninvasively, and without the use of any ionizing radiation or contrast agents. Living tissues have naturally a lot of water that contains protons. The behavior of these protons in the strong magnetic field can be observed with an MRI scanner. Magnetic resonance image is a contrast difference image that arises from the distinctive behavior of protons at high magnetic field in particular tissues.

Local indifferences in the tissue temperature carry a lot of information. Heat distribution of tissue can even be used in order to diagnose malformations such as tumors. Some diseases can be diagnosed based on the temperature of the tissue *in vivo*. Some conditions can be treated with temperature therapy. The examination of the tissue temperatures inside the body cannot be done noninvasively with conventional methods. Luckily, the shift of temperature changes the local magnetic properties of a tissue containing water, which can be observed with the MRI scanner. That is why MRI can be used as a guiding method in noninvasive temperature treatments, and also as a noninvasive diagnostic tool.

MRI scanner needs to use electromagnetic radiation and strong changing magnetic fields. In some cases, the use of these phenomena may lead to contraindication to MRI examination. It is obvious that no ferrous metal should be placed in the strong magnetic field. Additionally, non-ferrous conductive materials possess a risk of heating during the scan. A conductive object can act as an antenna or a resonating loop that picks up the energy from the used radio frequency radiation causing excessive heating. Again, living tissues are slightly conductive which is why a powerful changing magnetic field may induce eddy currents in them. By Faradays’s law, eddy currents try to create an opposing magnetic field against the

scanners field. When current flows through resistive tissues, Joule heating occurs. That is why it is utterly important to first test the MR compatibility of all the devices used and keep a watch of the possible tissue heating due to eddy currents. MRI scanner itself could be used to measure unwanted heating related to unordinary conductive components inside living tissues, and additional gadgets included in the MRI examination. These elements could include for example conducting implants or supplementary measuring devices used in MRI, especially in fMRI examinations, such as cameras, microphones, thermometers, pulse oximeters, electrocardiographic, or electroencephalography devices *etc.*

The MRI scanner can be used to follow the temperature of the tissues. There are few possible ways to produce heat information with MRI. Main ways to do so, are based on the observation of the diffusion, longitudinal relaxation and proton resonance frequency, or using spectroscopic methods or temperature sensitive contrast agents. Every method has its own pros and cons. From these, the proton resonance frequency (PRF) method is the industry approved golden standard for observing temperature with a MRI scanner.

The purpose of this thesis is to familiarize reader to the magnetic resonance thermometry methods and demonstrate the use of the proton resonance frequency method to produce volumetric thermometry data with an MRI scanner. This thesis explains the theory behind PRF method and explains how to optimize the examination to achieve the best possible temperature information.

Aalto NeuroImaging (ANI) is a research infrastructure that is part of the Department of Neuroscience and Biomedical Engineering (NBE) at Aalto School of Science. AMI Centre provides and maintains facilities and services for research-dedicated neuroimaging purposes, with modalities such as magnetoencephalography (MEG), navigated transcranial magnetic stimulation (nTMS), and magnetic resonance imaging. This thesis was done with ANI´s 3T whole-body MRI scanner: Magnetom Skyra, Siemens, in AMI Centre.

The structure of this thesis, is as follows: Chapter 2 gives an introduction to main points needed in order to understand the principles of MRI. Chapter 3 gives an insight to the magnetic resonance thermography and answers to the question why to perform thermographic examination with the MRI scanner. Chapter 4 presents the methods and instrumentation used to perform temperature measurements in practice. Chapter 5 illustrates the results that arose from the use of the MRI scanner for thermographic purposes. Last two chapters, 6 and 7 consists of the further discussion and the closure conclusion.

2 Magnetic resonance imaging

2.1 Magnetic resonance in MRI

Magnetic resonance imaging (MRI) is an imaging method based on the nuclear magnetic resonance (NMR) phenomenon. MRI scanner can detect subtle changes in the magnetism of the target nucleus. Water molecule consists of two hydrogens and one oxygen atom and make up 70% to 90% of most living tissues. The magnetic behavior of the hydrogen proton in water and in some fat molecules is observed in MRI. A proton has a magnetic spin and therefore it also possess a magnetic moment. Magnetic moment can be defined with classical mechanics as it describes the torque that a particle experiences in an external magnetic field. Exact description of NMR phenomenon would require quantum physics, but it is not required in order to understand the basic principles of an MRI scanner. MRI uses a strong static magnetic field that turns proton's magnetic moment according to the field. Some protons align parallel and some antiparallel to the magnetic field of a MRI scanner. Protons that are aligned parallel to the magnetic field have slightly lower energy state, and therefore are in a steadier state. The relation of antiparallel and parallel protons in a 3T field is roughly million to million and twenty two. These 20 ppm extra protons that are aligned parallel to the magnetic field produce the net magnetization that the MRI machine observes. The stronger the magnetic field, the bigger is the energy difference of these two proton types aligned in opposite directions. Larger energy difference leads to bigger proportion of protons aligned to the field direction.

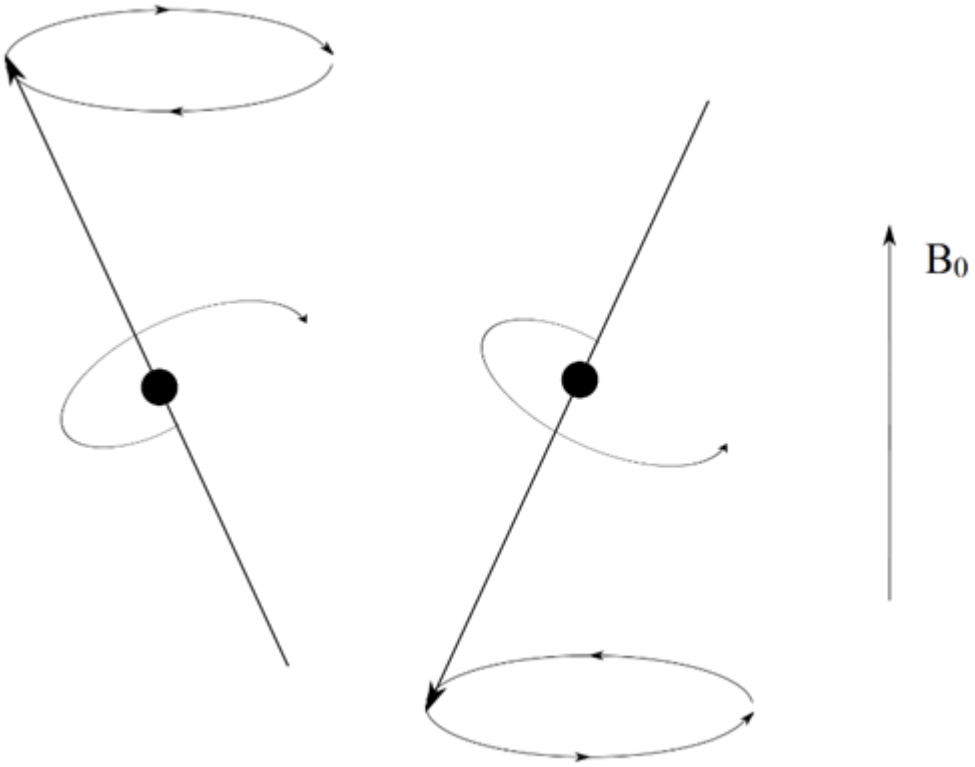

Figure 1 Spinning and precessing protons aligned parallel and antiparallel in magnetic field. All the figures in this thesis are done by the author with Inkscape, (Free Software Foundation, USA) or MATLAB (MathWorks, USA) softwares.

As illustrated in Figure 1, the protons are not directly aligned with magnetic field, but precessing around the parallel or antiparallel direction of it. Protons spin around their own axis which is the reason they have a magnetic dipole moment $\vec{\mu}$

$$\vec{\mu} = \gamma \vec{J} \tag{1}$$

where γ is the gyromagnetic ratio for proton, and angular momentum J is:

$$J = \hbar\sqrt{s(s+1)} \quad S = \frac{n}{2}, n = 1,2,3 \ldots \tag{2}$$

Where s is the spin number, which is either integer or half integer, and $\hbar$ is the reduced Planck's constant. Angular momentum makes the proton precess around the direction of the external magnetic field. Stage in Figure 1 is the initial stage at MRI scanners magnetic field, before an excitation pulse is applied. Proton precessing around the magnetic field direction has a spin of +1/2, and proton precessing around the opposite direction has a spin of -1/2.

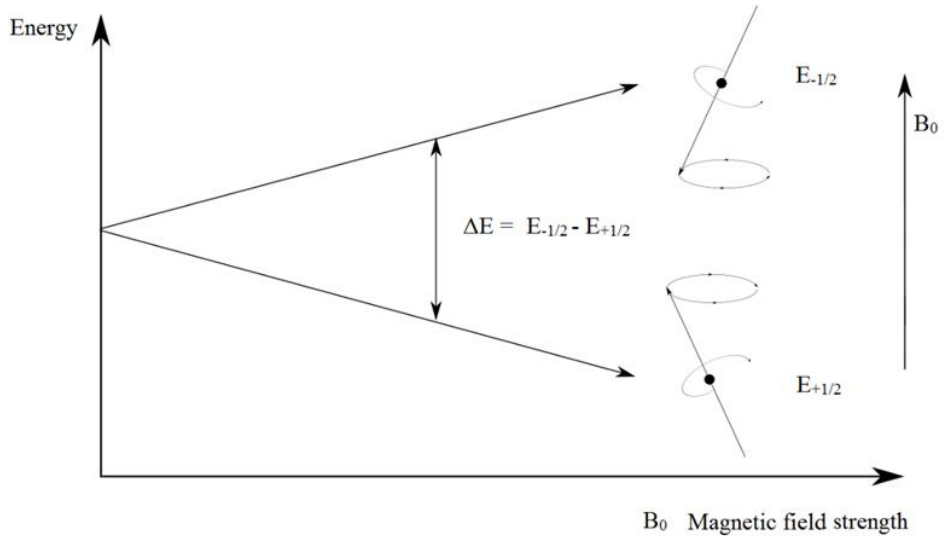

Figure 2 Protons aligned in the direction of magnetic field have a slightly lower energy state than the antiparallel ones. Extra amount of these parallel protons generate the net magnetization that is examined in the MRI.

The difference in the amount of turned protons can be detected from energy level difference

$$\Delta E = \frac{\gamma h B_0}{2\pi}, \tag{3}$$

where γ is proton's gyromagnetic ratio for proton, B_0 is external magnetic field of the scanner and h is the Planck's constant. The relation of the parallel N_p and the antiparallel N_a proton spins as a function of the magnetic field can be solved from the Boltzmann statistics rules as

$$\frac{Np}{Na} = e^{(\frac{\gamma h B_0}{k_B T})}, \tag{4}$$

where k_B is the Boltzmann's constant and T is the room temperature in Kelvins.

In Figure 2, the energy difference of protons in strong magnetic field is illustrated. Magnetic resonance imaging is based on the examination of the few extra protons aligned parallel to the scanners field. Protons aligned in opposite directions cancel out each other spin magnetic moment, which is why few extra parallel align protons are needed.

When talking about protons in MRI, one is usually referring to the few extra parallel align protons. These extra protons produce the net magnetization of the tissue. By disturbing these protons with a radio frequency (RF) pulse that tilts the net magnetization, and observing the net magnetization to go back in initial stage with the magnetic field, we can study the differences in chemical environments at the target tissues containing protons.

The MRI scanner's RF pulse has a specific Larmor frequency

$$\omega_0 = -\gamma B_0, \tag{5}$$

which targets unique nucleus determined by the gyromagnetic ratio, in this case proton. The gyromagnetic ratio γ for proton is approximately 42,577 MHz/T and it is the amount of loops a proton precess in 1s at 1T. The Larmor frequency is the only frequency that a proton can sufficiently absorb energy. Magnetic field strength B_0 for a clinical MRI scanner is usually 1,5T or 3,0T. The direction of the scanner's magnetic field is the Z-direction, and it goes through the main tube. RF pulse is polarized so that the force that 90° RF pulse induces to the protons will turn the net magnetization to the XY-plane. Early RF coils in MRI were linearly polarized, but nowadays almost all coils, transmit and receiving, are circular polarized.

Different tissues have different magnetic properties *e.g.* due to different water concentration. After the tilt, net magnetization M_0 goes simultaneously back in the initial stage with two different ways. The phenomenon is called magnetic relaxation and the two different relaxation types are called T_1 and T_2 relaxation. The T_1 value describes the relaxation in Z-axel direction. The T_2 value represents the speed of the transversal relaxation.

2.2 Relaxation times T_1 and T_2

The T_1 value describes the time it takes the M_0 to gain back approximately 63% (1-(1/e)) of its initial value in Z-axel direction. The T_2 value describes the time it takes the M_0, that is flipped to the XY-plane, to decay to approximately 37% (1/e) of its full strength. These relaxation times from recovery and decay are illustrated in Figure 3. T_1 relaxation time can be described with the help of M_z, the vertical part of the net magnetization as:

$$M_z(t) = M_{z,0}(1 - e^{-t/T_1}), \tag{6}$$

where $M_{z,0}$ is the part of the initial net magnetization in the Z-direction. T_2 relaxation time can be described with the transversal part of the tilted net magnetization (M_{xy}).

$$M_{xy}(t) = M_{xy,0}e^{-t/T_2} \tag{7}$$

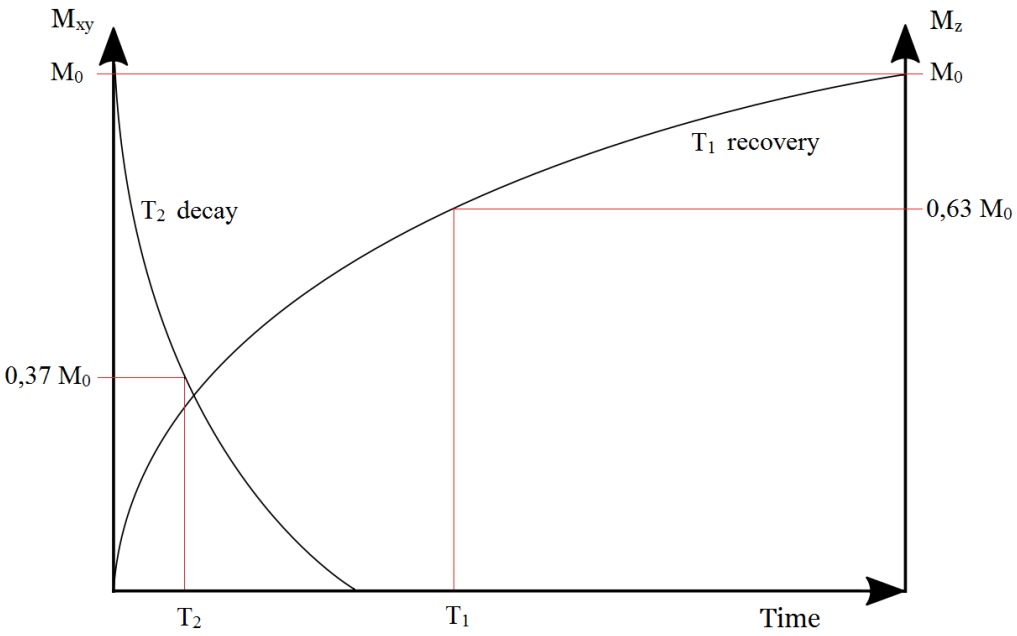

Figure 3 T_1 – time at 63% recovery and T_2 – time at 37% decay

In Figure 4, T_1 and T_2 relaxations are visualized in Cartesian coordinates. These relaxations occur simultaneously, but it is easier to examine them separately. T_1 relaxation, clarified in Figure 4.a), happens in z direction due to the MRI machine's static magnetic field B_0 and is also called spin-lattice relaxation. T_2 relaxation takes place in XY-plane and is again called spin-spin relaxation. Spin-lattice or T_1 relaxation refers to the relaxation process that is lattice or surroundings induced. In T_1 relaxation, the medium containing observed protons goes towards the thermal equilibrium. T_2 relaxation occurs mainly because of the dephasing of the precessing spins, illustrated in the Figure 4b. Dephasing speed is related *e.g.* to the size of the surrounding molecules. Fat has bigger molecules than water, and has thus faster spin-spin relaxation speed and shorter T_2 time than water.

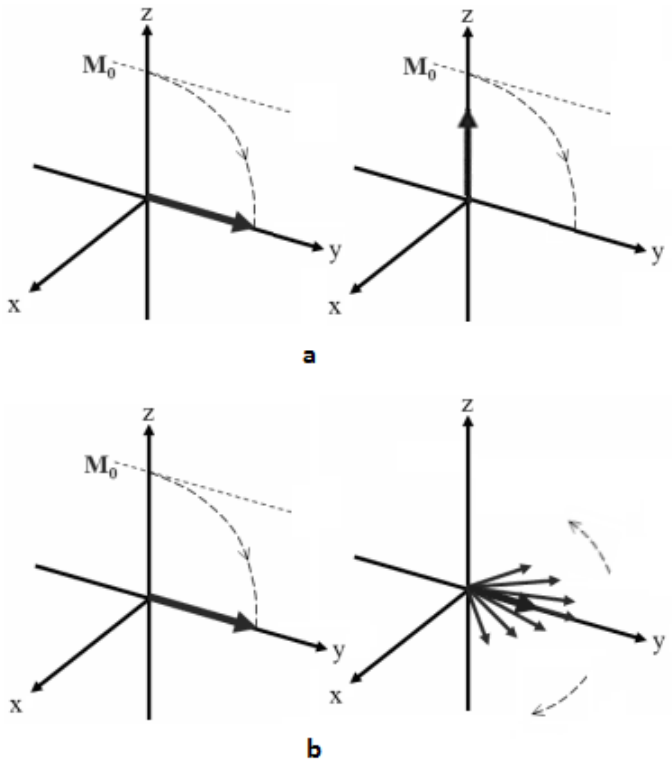

Figure 4. a) T_1 relaxation is the time when ~63% of M_0 is gained back in Z-direction b) T_2 relaxation is the time when ~37% of the tilted M_0 is left in XY-plane.

In reality, there is always magnetic inhomogeneities, which accelerate the transversal relaxation time T_2 such a way that

$$\frac{1}{T_2^*} = \frac{1}{T_2} + \frac{1}{T_2^i}, \tag{8}$$

where T_2^* is the actual relaxation time and T_2^i originates from the presence of the surroundings. That is why in MRI studies where the lateral relaxation is observed, the T_2^* is used instead of T_2.

Particular types of tissues have distinctive relaxation times due to different magnetic properties. Different and changing magnetic properties can be observed with MRI to create an image or to investigate chemical composition of tissues. The magnetic properties and amount of water changes in different conditions like trauma and diseases, which makes MRI also a sensitive clinical diagnosing tool. MRI creates a contrast difference images that displays the differences in chemical properties of targeted nucleus and tissues. That is why MRI is a good tool for detecting changes. Changes in magnetic properties in tissues can be rooted from *i.e.* temperature changes.

2.3 Imaging parameters of the scanner

In magnetic resonance imaging, a person operating the scanner, can change imaging parameters in order to achieve a desired outcome. Main imaging parameters that are regularly changed are echo time (TE), repetition time (TR) and flip angle (FA). Other common changeable values are for example the scanning direction, field of view (FOV), slice thickness, and matrix size that denotes how many data points are collected in a slice.

TE and TR values define the temporal characteristics of the reading of the observable signal originating from the magnetic relaxation process. FA describes the direction, in degrees from the Z-axel, of the applied RF pulse. The echo time, or time-to-echo, is the time between the initial RF pulse and the examination of the MR signal. Repetition time, or time-to-repeat, is the time in which the examination is repeated, meaning that a new RF pulse is applied and a new echo is recorded. By changing TE, TR and FA one can decide the contrast of the target tissues in the final image.

If the echo time and repetition time are long, it usually means that the major part of the signal from the relaxation originates from the lateral relaxation. If the signal is mainly from the later relaxation we say that the image is T_2 weighted. In T_2 weighted images, fluids, for instance blood, are seen bright. Fat consists of big molecules, and have thus fast spin-spin relaxation speed and short T_2 time. If the TE is long, signal from the fat relaxation have already gone. That is why the signal from the fat is not as bright as signal from the water in the T_2 images.

If the TE and TR are short, the detectable signal is primarily from the longitudinal relaxation. If most of the signal is from the longitudinal relaxation process, the image is called T_1 weighted image. T_1 weighted images show bright signal from the fat tissues, because fat starts quickly to align back to the equilibrium stage. If the signal is recorded at the time when the fat emits lots of signal, fat is seen bright in the image.

In conclusion the timing of the signal examination can alter the brightness of the tissue in the final magnetic resonance image. The specific TE, TR and FA, among other changeable imaging parameters, are saved for specific time series called pulse sequences. Different type of sequences are used to emphasize or lose signal from the desired tissue types.

2.4 Spin and gradient echo

The observable signal originating from the magnetic relaxation of net magnetization after the excitation pulse is called free induction decay (FID). In MRI, there is two basic principles to observe the free induction decay. These two basic pulse sequences are called spin echo and gradient echo. Pulse sequence is a time series that describes the use of radio frequency and gradient coils. Radio frequency coils in the bore of the magnet emit a circularly polarized electromagnetic pulse that can tilt the net magnetization in desired direction. Gradient coils in the magnet tube create magnetic fields, in addition to the static magnetic field created by the main magnet. The magnetic fields generated by gradient coils are needed in order to get the spatial distribution of protons.

Spin echo is formed with a refocusing 180° RF pulse after the first 90° pulse. The 180° pulse rephases the dephased magnetization in XY-plane. 180° pulse is applied at the half point of the echo time or time-to-echo (TE) as seen in Figure 5. After the initial 90° pulse, the net magnetization is turned to the XY-plane as illustrated in Figure 4.b). Then the magnetization immediately starts to dephase in the XY-plane. The purpose of using the 180° pulse is to get the XY-magnetization back to the same phase by the time it is recorded (TE). The center of the time point when the spin echo is recorded is the stage when no lateral magnetization exists, or it is on the X-axel. Spin echo pulse sequence is presented in Figure 5. Usually a spin echo emphasizes the T_1 relaxation of the net magnetization. The reading of the FID in spin echo can be timed so that the XY-component of the FID is symmetrically eliminated, in other words, no signal arosing from the dephasing of the net magnetization is recorded. This kind of spin echo records a FID signal that originates entirely from the vertical spin-lattice relaxation process and has no signal from the lateral relaxation because of timing of the applied 180° RF pulse, which destroys the lateral magnetization. The spin echo sequence, with different timing, can also be used to emphasize the lateral relaxation, but the 180° RF pulse cancels the T_2^* relaxation arising from dephasing due to magnetic inhomogeneities of surroundings, such as temperature changes. The neutralization of the lateral relaxation in spin echo is further portrayed in Figure 6.

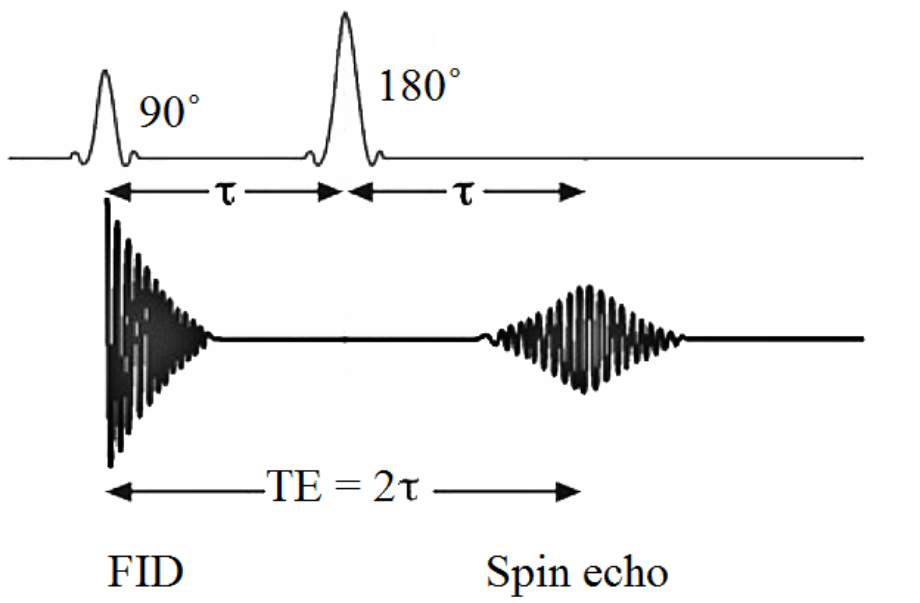

Figure 5 Spin echo sequence where the timing of the 180° pulse removes the signal from the lateral relaxation.

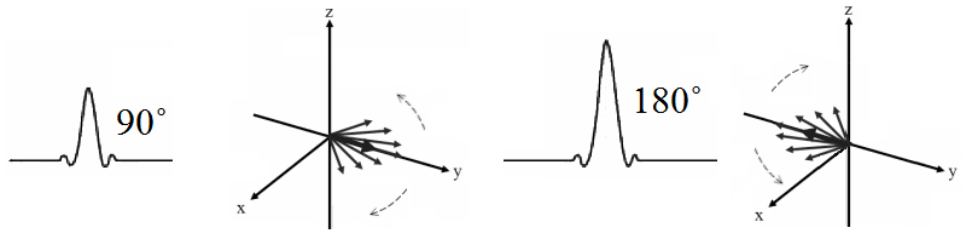

Figure 6 The neutralization of the lateral part of the FID. The FID is recorded symmetrically around the point TE, when the spins are aligned with the x-axel. To simplify the picture, no vertical part of the magnetization is shown.

Gradient echo differs from spin echo in that manner that it uses the fact that protons at different locations in the target tissues get out of phase at distinctive pace. It means that gradient echo does not try to rephase the magnetization in the XY-plane but is based on the speed of lateral relaxation. Gradient echo includes the use of a frequency encoding gradient (G_F) seen in Figure 7. The G_F gradient is used to artificially speed the dephasing of the spin frequencies. As a result, FID is lost much more quickly than through normal relaxation process. When reversibly polarized gradient GF+ is applied proton spins start to get quickly back in phase. When the FID is read around the point where the lateral part of the net magnetization is back in phase, we get strong lateral signal. This is because when magnetization from the protons are aligned at the same phase, it is easier to examine them to get out of phase. Otherwise, the lateral relaxation of the magnetization is greater with protons that are already at the same phase. The name of gradient echo comes from the described use of the gradient. Gradient echo method collects

FID signal that majorly consist of lateral part of the net magnetization. The method is so quick that the vertical relaxation does not have much time to develop. Gradient echo is a good method to emphasize the tissue characteristics which are related to the lateral relaxation process due to dephasing of spin frequencies.

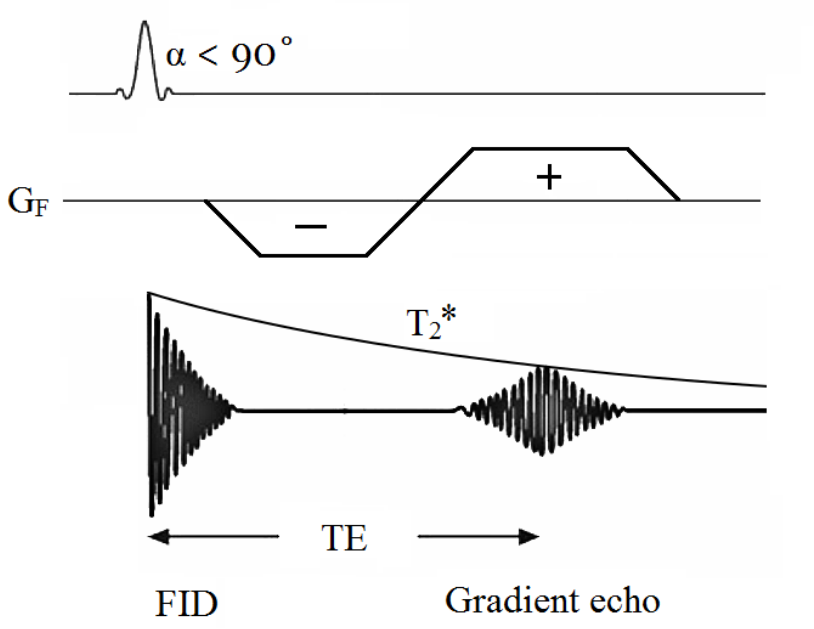

Figure 7 Gradient echo sequence, where frequency encoded gradient G_F is used to bring up the dephasing relaxation effects of the surrounding tissues. First G_{F-} gathers transversal net magnetization components to the same phase, then G_{F+} is applied during the read out of the FID. The change of phase is now fast during the read out, which leads to great amount of phase information from the target.

Gradient echo can be used much faster than spin echo. In addition to the use of G_F also flip angle smaller than 90° is used in RF pulse. Smaller flip angle of the net magnetization and short echo time can be used, because gradient echo does not need a RF pulse that refocuses effect of main field inhomogeneity. Vertical relaxation is limited with short echo times, which means that gradient echo sequence is mainly based on the transversal relaxation.

3 Magnetic resonance thermometry

3.1 Body temperature and MRI

In the hunt for better signal-to-noise (SNR) quality, high field MRI machines have become more common. Many routinely practiced MRI procedures at low field may not be allowable at higher field strengths, due to overly vast specific absorption rate (SAR) for radiofrequency power. These SAR regulations are there for to prevent excessive heating of patient during MRI examination. Also many low field safe utensils and implants may not be high field safe due to the heating problems. The heating challenge at high field strengths has led to the evolution of temperature measuring methods in MRI. Physical temperature measuring devices can only measure temperature from the very surface of patient, the part where patient already has temperature sense. Additional temperature measurement devices also has to be build MRI safe, for example non-metal parts such as optical fibers may need to be used.

Body temperature is closely related to various physiological functions. By observing temperature distribution in the body it is possible to diagnose disorders related to metabolic abnormalities. In extreme cases the body temperature can be used even to locate tumors by observing temperature recovery process after heating or cooling of the body [7]. Temperature mapping could also be used *i.e.* for cardiac studies during and after cardiac surgery. Temperature mapping is also crucial in many thermal therapies.

Much interest has recently been focused on hyperthermia treatments with using laser, microwave, radiofrequency, infrared, or ultra sound heating methods. Hyperthermia treatments can be used for variety of medical interventions including tissue architecture studies, tumor ablation, drug delivery *etc.* [2, 7].

3.2 Benefits and challenges of MR thermometry

Thermal therapies such as hyperthermia and thermal ablation are used as a treatment method for various diseases and tumors. Thermal ablation methods are preferred to surgical methods because they can be repeated numerous times, are less invasive and do not do so much damage to secondary tissues. It is goal to achieve a sufficient temperature change in the target tissue in order to produce irreversible damage for *i.e.* tumor. That is why a precise thermal mapping is desired during thermal therapy. When heating tissues, multiple physical and physiological processes occur. Practically speaking it is hard to define a single threshold for tissue damage. During thermal therapy it is crucial to measure temperature not only from target tissues but also from surrounding tissues to protect unwanted tissue damage *e.g.* due to coagulation. Because of the measurement method and tissue related uncertainties usually two tissue areas need to be specified: one in which the thermal exposure will be far above the damage threshold, and one other distant area in which thermal exposure must stay far below the safety threshold.

General scenario where the NMR temperature imaging could be used as a guiding method would be a thermal ablation of a tumor. MRI-based temperature measurements include numerous sources of uncertainty factors including noise, error in baseline temperature, the effects of averaging the temperature over several voxels, calibration of the MR thermometry method *in vivo*, drift of the static magnetic field, motion or tissue swelling induced artifacts [23].

In MRI examinations there is a possibility of notable heating and patient burns. These kinds of thermal injuries can happen due to electromagnetic induction heating or antenna effect of a conducting article [35-40]. Induction heating could occur when a conducting loop is formulated in the imaging region where the time-varying gradient magnetic fields and RF pulses are used. Other possible heat injury scenario would be when for example monitoring cable could act as an antenna picking up the used RF signal frequency. The electric field induced by the currents has a maximum field line density at the tips of the antenna [36]. A pulse oximeter within scan area could act as an antenna in high power scan, and the tip attached to the finger could lead to burn injury. In a 3T MRI machine such an antenna would be approximately 1,2m long in air. The possibility of heating is maximized for conducting objects with the length in the range of an odd number of half wavelengths of the RF field [39]. Important aspect of the antenna effect is the surrounding tissue properties. Electrical permittivity of the tissues change the operating RF pulse wavelength in the tissue which shortens the length of a con-

ducting element which could act as an antenna. For example in muscle tissue approximately 13cm wire in 3T MRI could act as an antenna. That is why it is important to test the heating of every kind of conducting elements used in a MRI studies.

MR thermometry is an effective way to map the temperature changes in tissues. Thermal guiding with NMR have been used with thermal therapy methods such as radio frequency, laser, ultrasound and microwave. If the thermal therapy duration is longer than few seconds it becomes hard to predict how different tissues heat up. Tissue properties such as energy absorption rate, perfusion and fluid flow have an influence to thermal distribution.

MRI can be used to measure temperature change due to temperature dependent variables. These variables include equilibrium magnetization M_0, diffusion coefficient D, spin-lattice T_1 relaxation time and proton resonance frequency (PRF) [15]. The temperature dependence of these variables can vary between tissues and organs. From these techniques PRF is the only one that does not suffer from major heat-induced changes. PRF method has become the golden standard in NMR-temperature imaging. NMR thermal guiding is rather sensitive to temperature changes so that it can also be used as a planning method in thermal therapies. The correct positioning of used transducer can be tested with slight temperature increase with no therapeutic effect, but enough to be seen in the MRI.

3.3 MR thermometry modalities

3.3.1 Proton density

Proton density has a linear correlation on the equilibrium magnetization, M_0, which is determined according to the Boltzmann distribution:

$$M_0^{PD} = \frac{N\gamma^2 h^2 I(I+1)B_0}{3\mu_0 kT} = \chi_0 B_0, \tag{9}$$

where N is the number of spins per volume, γ is the gyromagnetic ratio, h is the Planck's constants, I is the spin number of proton (1/2), B_0 is the magnetic field strength, μ_0 is the permeability of vacuum, k is the Boltzmann's constant, and T is the absolute temperature. The susceptibility χ_0 can be derived from the Curie law:

$$\chi_0 = \frac{1}{T} \tag{10}$$

Temperature changes can be estimated from the change of signal intensity of proton density-weighted images. The seen change of the proton density originates from the temperature sensitivity of the magnetization. The change in the equilibrium magnetization affects the ratio of the parallel and antiparallel protons, and that is why it is detected as a change of proton density. Of course the actual proton density of the tissue remains the same, but the relative change of detected proton density due to changing temperature can be observed.

The temperature sensitivity of the proton magnetization is around -0,30 ± 0,01%/˚C between 37˚C to 80˚C [2], which is the temperature range commonly inspected in MR guided thermometry of living tissues. The temperature sensitivity of the proton density thermometry method is quite small, and that is why a high signal-to-noise ratio (SNR) is required. A SNR of 100 would lead to temperature uncertainty of 3˚C. Also long repetition times are needed in order to eliminate the effects arising from the T_1 relaxation time. If fast MRI techniques are used it comes harder to distinguish what are the basis of the observed signal change, relaxation time changes or proton density changes.

3.3.2 Diffusion coefficient

First MRI temperature mapping based on molecular diffusion was introduced in 1989 by Bihan et. al. The method was first used in guidance of clinical hyperthermia and was found to be more accurate than MR thermometry based on T_1 relaxation [65]. It is based on the tissue water diffusion originating from thermal movement. Thermal Brownian motion of molecules is described by the diffusion constant D. The relation between temperature and the diffusion constant is exponential:

$$D \approx e^{-E_a(D)/kT} \tag{11}$$

Where E_a is the activation energy, k is the Boltzmann constant, and T is the temperature. The diffusion constant temperature dependence can be described as:

$$\frac{dD}{DdT} = \frac{E_a(D)}{kT^2} \tag{12}$$

Diffusion of water has considerably higher activation energy than T_1 relaxation, about 0,2eV. The change in diffusion coefficient amounts for roughly 2% / ˚C. [2]

Diffusion was first measured with MRI in 1965 by Stejskal *et al.* [66] by observing spin-echo signal attenuation in the presence of a time-dependent field gradients. The signal depletion in diffusion-weighted images originates from the dispersion of acquired signal phases proportional to the distribution of displacements. The signal intensity lowers from diffusion and can be described as signal attenuation:

$$FID = FID_0 e^{-\gamma^2 G^2 \delta^2 \left(\Delta - \frac{\delta}{3}\right) D}, \tag{13}$$

where G is gradient strength, δ is duration of gradient pulse, and Δ is time between the two gradient pulses. When temperature variations are small and the E_a is independent of temperature, the temperature change in two images can be mapped from equation:

$$\Delta T = T - T_{ref} = \frac{kT_{ref}^2}{E_a(D)} \left(\frac{D - D_{ref}}{D_{ref}}\right) \tag{14}$$

Diffusion has a good temperature sensitivity but it has practical problems for *in vivo* studies. Problems occurs when the mobility of the water is determined by the cell structures of tissues rather than the heat distribution. That is why diffusion based MRI is more often used to determine tissue structures such as blood vessels and nerve pathways, rather than heat distribution. Diffusion based temperature mapping needs multiple measurements which extends the measurement time. Diffusion based thermometry suffers from extremely high sensitivity to motion. Although motion sensitivity of diffusion method can be reduced with line-scanning techniques. Single shot MRI-techniques like EPI can be used to reduce motion sensitivity [1]. Field dependence of the diffusion based MR thermometry is negligible [2].

3.3.3 T1 relaxation constant

T_1 relaxation time can be used to measure temperature changes in tissues. Although the temperature sensitivity of the T_1 relaxation time is tissue dependent.

First reported temperature mappings made with MRI in 1983 were based on T_1 relaxation time [65]. T_1 relaxation has advantages such as it is not so sensitive to motion and it can also be used for fat tissues contrary to for example proton resonance frequency (PRF) method. T_1 relates to the temperature by following affinity:

$$T_1 = T_1(\infty)e^{-E_a(T_1)/kT}, \tag{15}$$

where $E_a(T_1)$ is the activation energy, and T is the absolute temperature. Temperature dependence of T_1 relaxation time is tissue dependent and therefore the dependence for each tissue must first be estimated. Of course also T_1 relaxation time is tissue dependent. The temperature dependence of T_1 can be noted as:

$$T_1(T) = T_1\left(T_{ref}\right) + m \cdot (T - T_{ref}), \tag{16}$$

where m is the temperature dependence of the longitudinal relaxation time. T_1 weighted image depends linearly on the net magnetization on protons, which is also temperature dependent. The nonlinear part of temperature dependence of the net magnetization is usually neglected within T_1 thermometry method. The magnitude image signal strength S is used to formulate the T_1 temperature dependence:

$$\frac{dS}{dT} = m \cdot \frac{dS}{dT_1}\left(-\frac{S}{T'}\right), \tag{17}$$

where the value inside the brackets is the nonlinear part of the net magnetization.

In vivo MR thermometry based on T_1 relaxation time has proven to be difficult because of the perfusion changes during cooling and heating [1].

3.3.4 Proton resonance frequency shift

The temperature sensitivity of the proton resonance frequency was first observed by Hindman in 1966 [33]. Temperature sensitivity PRF thermometry has provided significantly better accuracy than diffusion method during *in vivo* experiments. PRF method has significant advantages. It needs no special hardware and standard gradient-echo sequences can be used. PRF thermometry method has

also a fast acquisition time when fast gradient-echoes are used [1]. The excellent linearity and independence with respect to tissue type [58], together with good temperature sensitivity, make PRF-based temperature MRI the preferred choice for many applications at mid or high field [2]. PRF-shift thermometry is currently only reliable MRI-based temperature measuring method *in vivo* [8, 12, 20, 21].

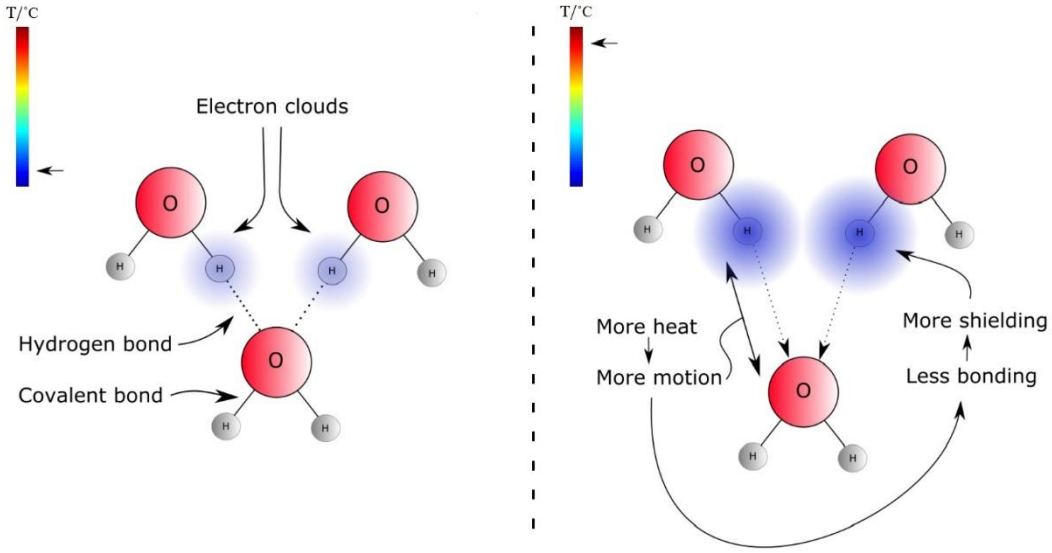

Figure 8 When temperature rises in water molecules, the hydrogen bonds get weaker. In the sketch, right side is hotter. Shielding effect of hydrogen electron clouds increases when hydrogen bonds are weakened. The electron cloud is of course around the whole molecule, and this is simplified illustration.

When temperature rises, the strength of hydrogen bonds of water decreases due to the increased motion of water molecules. Lowered hydrogen bonding leads to bigger screening effect of the electron clouds. Screening effect has an influence to the proton's local magnetic field. And when the local magnetic field is lowered the phase difference occurs.

The increase in water's electron cloud shielding due to the temperature rise is illustrated in Figure 8. The right side of Figure 8 represents the water molecules after heating. More heat means more motion, which is thought to bend, brake, and stretch the intermolecular hydrogen bonds. Electrons make up the hydrogen bond, so when the electrons are rotating more over the hydrogen, not the bond, it means they have more shielding effect towards the surrounding magnetic field. This way temperature change can induce phase shift in MRI *via* the increased electron cloud shielding of the examined water protons.

It should be noticed that the temperature induced phase shifts are TE dependent, which means that the TE used during the temperature measurement should remain constant. This echo time temperature dependence is linear, and is illustrated in Figure 9. The echo time could be determined so that the measured temperature range leads to sufficient phase shift. If the echo time and temperature change is very small, the expected phase shift would be really small and thus hard to detect. In the other hand, if the time to echo is rather long and examined temperature change is broad, the temperature change could even wrap the phase which is inconvenient.

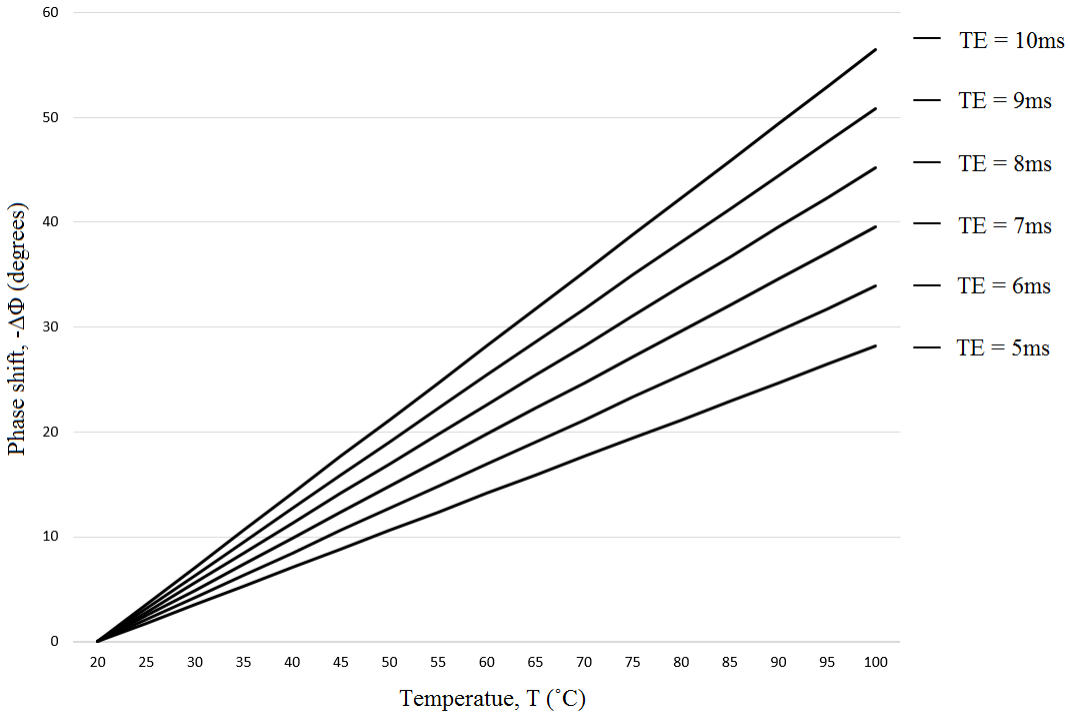

Figure 9 Phase shift temperature dependence with different echo times (TE). Starting temperature is set to 20˚C and temperature sensitive coefficient α = -0,01ppm. Vertical axel describes the phase shift in negative direction, as α is negative.

For *in vivo* experiments the temperature in the magnet bore can increase due to the body temperature, which can even change the image phase. *In vivo* experiments include also other sources of phase variations like perfusion and changes in the oxygenation level of the blood. Susceptibility of the blood is function of the oxygenation level and susceptibility changes have an effect to the local magnetic flux density. Susceptibility changes have that way also an effect to the magnitude of proton resonance frequency shift. The phase of the muscle tissue decreases when it is cooled. This corresponds with the behavior of pure water. The phase of fat increases when fat is cooled. That illustrates that fat does not behave like pure water.

Temperature change ΔT can be calculated from the phase difference using equation,

$$\Delta T = \frac{\Delta\Phi}{\alpha \cdot TE \cdot (\gamma B_0)}, \tag{18}$$

where TE is the gradient echo time, and α is the temperature sensitivity chemical shift coefficient of tissue water. The phase difference SNR correlates directly to the signal intensity:

$$SNR_{\Delta\Phi} \triangleq |\, \Delta\Phi(\Delta T)\,| \cdot A, \tag{19}$$

where A is the signal intensity, which is dependent on the tissue parameters T_1, T_2^* and the sequence parameters TE, TR, and FA [17].

PRF method can be used by taking two identical set of magnitude and phase images in different temperature conditions. Phase difference images can be processed in the following two ways. First one uses the raw data, so that the files from the baseline and the reference image are Fourier transformed after bilinear interpolation to square matrix. In the complex image space, the signal in a single pixel is described by $M_1 \cdot e^{i(\omega\tau+\Phi)}$ [35]. Pixel-by-pixel division of the baseline image by reference image yields:

$$\frac{M_1 \cdot e^{i(\omega\tau+\Phi)}}{M_2 \cdot e^{i(\omega\tau+\Phi+\Delta\Phi)}} = \frac{M_1}{M_2} e^{-i(\Delta\Phi)} \tag{20}$$

Performing the operation,

$$arctan\frac{M_1}{M_2} \cdot e^{-i(\Delta\Phi)} = \Delta\Phi \tag{21}$$

for complex images, returns the phase difference. Complex image method has the advantage of not having the wrapping problem of the phase images. Although the scanner does diverse signal processing to the raw data to create the magnitude and the phase images [25], which have to be done manually when the raw data is used.

Second way to produce phase difference images is simply to use the magnitude and phase images the scanner reconstructs from the raw data. In practice, any gradient echo sequence can be used to produce phase images, because gradient echo sequences do not have the refocusing pulse that removes the temperature induced error in the lateral relaxation. Spin echo sequence has the 180° refocusing pulse in the XY-plane which gets rid of the signal that is needed in order to define the temperature change from phase shift. If the scanner's magnitude and the phase images are used, the challenge is to get the phase images unwrapped acceptably, and to remove the possible error due to the magnetic field drift.

Downside of the PRF method is that it has high demands on the external magnetic field stability. The drift of the external magnetic field during temperature mapping will enhance the temperature related changes. The drift of the magnetic field happens always when the scanner is used. The magnitude of the magnetic field drift for a 3T scanner can be about 0,05ppm/h for a spherical volume of 20cm diameter. When the PRF method is based on the water chemical shift which is about -0,01ppm, it means that in the worst case, field drift can cancel out the temperature induced phase shift in 12 minutes. The field remains most stable in the center of the image, but the field change can lead to error in the temperature measurement at the edges of the object imaged. The field drift happens mainly because the use of the gradient coils induces eddy currents to the passive shim components of the magnet. These passive shim components are not within the cooling system of the scanner, so they can heat up due to the Joule heating. The passive shim elements can consist *e.g.* of small pieces of sheet metal or ferromagnetic pellets [69]. These sections of the scanner try to create opposing magnetic field which induces current in opposite direction to the current induced by the gradient coils. The static shimming changes when the passive shimming components heat up, which leads to field drift, especially in the Z-direction of the tube.

Active shimming could be used prior to the using of the PRF MR thermometry method in order to get the most accurate temperature measurement. The mean drift of the magnetic field can be corrected using an external reference phantom that remains at fixed temperature during the scan. The magnetic field drift can also be first measured with PRF method, and later reduced from the actual PRF temperature measurement. In some *in vivo* cases it could be also possible to use fat tissue as a reference because fat does not experience same kind of temperature sensitive proton resonance frequency shift as water does [3]. The PRF-temperature relation in fat tissue occurs almost completely due the susceptibility effects [4]. Magnetic field drifting problem and susceptibility changes can be neglected using the fat's chemical shift as an inner temperature reference [11]. Absolute temperature can also be measured using a fat as a reference for water. Fat's

chemical shift does not change when temperature changes because it has no hydrogen bonds. Although, if the fat's chemical shift is to be used, it could be wise to just use the spectroscopic MR thermometry method. Finally, it is also possible to use multi-baseline methods to reduce the error from field drift [5].

3.3.5 Spectroscopy

Previously described MR thermometry methods based on either the proton density (PD), diffusion coefficient (D), T_1 relaxation time, or proton frequency shift (PRF) only accounts for relative temperature changes with the comparison of two identically acquired images. When just two images are compared together, no absolute temperature can be determined. Spectroscopic MR thermometry is in that way unique imaging method that it is able to measure the absolute temperature. It is based on the same kind of phase shift of the protons as the PRF method, but the frequency shift is calculated from the MR spectra [17]. The proton resonance frequency shift is calculated using the water proton peak and a reference peak that remains stable when the temperature is changed. Because the frequency shift is determined with such spectral studies, the spectroscopic method is also termed chemical shift imaging (CSI). Such stabile substances in living tissues which do not experience a temperature induced frequency shift would be *e.g.* lipids and N-acetyl-aspartate (NAA) in the brain. When using this kind of additional internal reference, the field drift problem of PRF methods is almost completely abolished. When a known reference is used, the chemical shift temperature measurement has a very high temperature sensitivity [9,10].

CSI methods require a rather complex analysis of the spectroscopic data. For example zero filling, filtering, modeling of eddy currents, peak fitting are vital, and also water suppression is needed for the sake of avoiding water and fat peak overlapping. The use of various heavy signal processing and sequence altering methods may lead to reduced SNR and temporal resolution. The greatest downside of the spectroscopic method is the long acquisition time in order to get good spatial resolution. The CSI method usually requires a scanning time of minutes in order to obtain data with acceptable SNR [10]. It is also possible that water and the reference substance may not be located near each other, which may lead to undesired susceptibility effects due to the difference in the local magnetic field. Spectroscopic temperature measurement methods also cannot be used in phantom studies where the phantom is filled with homogenous material containing nothing to use as a reference. In phantom studies, spectroscopic methods would also require phantoms with special materials such as contrast agents.

3.3.6 Contrast agents

Temperature-sensitive contrast agents can be used to boost the temperature sensitiveness of the PRF based spectroscopic temperature studies. These include paramagnetic liposomes, paramagnetic lanthanide complexes, and spin transitional molecular materials [17]. For example some lanthanide complexes have over 10-60 times higher temperature sensitivity than water proton [9]. Although theirs toxicity limits the amount of the dose in biological tissues to maximum $1mM$.

Paramagnetic liposomes are made by combining a gadolinium or manganese compound and a phospholipid. Phospholipids generate a membrane which have a unique phase transition temperature (T_m). Under a certain phase transition temperature, the membrane does not allow water exchange through the lipids. Above the particular T_m temperature the contrast agent's membranes become permeable leading to the rapid relaxation agent flow to the surrounding tissues. The T_m of the phospholipid can be controlled by varying the length and saturation of the hydrocarbon chain [17].

Spin transitional molecular materials are molecular complexes which have a different stabile spin that switches by its chemical composition. The chemical composition of these molecules are temperature dependent [61], and that is why they can be used for temperature measurements in MR studies. Interest have been on the use of contrast agents which are based on the change of the ferromagnetic substances ability to stay ferromagnetic in the external magnetic field [62].

These kinds of contrast agents does not necessary allow a continuous temperature measurement, but can be used for a precise one time temperature measurement of the desired threshold. The temperature is measurable for couple of minutes. Paramagnetic temperature sensitive contrast agents can also be used for a local drug delivery. That is why these kinds of contrast agents can also be used in the MR guided drug delivery. The future of the MR thermometry based on contrast agents lies mainly on the discovery of new non-toxic contrast agents.

4 Materials and measuring methods

4.1 Instrumentation

4.1.1 MRI-system

Magnetic resonance imaging experiments were performed on a 3 T MAGNETOM Skyra whole-body scanner (Siemens Healthcare, Erlangen, Germany), using a standard receiving 32-channel head coil. The magnet is a 173cm long and 70cm wide open bore magnet with a mobile patient table. The operating software was Syngo MR D13C. The main magnet is there to generate the static magnetic field needed to polarize the hydrogen nuclei in the target. Shim coils and iron plates are used to guarantee the spatial homogeneity of the magnetic field in the magnetic bore. Shim coils are said to yield the active shimming, and the iron plates are said to cause passive shimming. Cylindrical gradient coil is used to create linear gradient field. Inside the gradient coil there is the RF coil which is used to transmit and receive RF pulse to excite and read the spins in the target being observed. [69]

Table 1. Homogeneity of the Siemens Skyra 3T magnetom magnetic field in the isocenter of the bore according to the manual. DSV stands for diameter of spherical volume.

Homogeneity		
	Guaranteed	**Typical**
10 cm DSV	0,01 ppm	0,003 ppm
20 cm DSV	0,05 ppm	0,03 ppm
30 cm DSV	0,30 ppm	0,20 ppm
40 cm DSV	1,40 ppm	1,20 ppm

The guaranteed and typical homogeneities for different size objects, in the magnet used in the examinations, are listed in Table 1. The drift of the main static magnet field is stated with ppm/h. For example a 20cm diameter spherical volume (DSV) in the center of the bore would have typically 0,03 ppm change in the magnetic field inside the object in an hour. It should be noted that the PRF thermometry has a sensitivity of about -0,01ppm. The inhomogeneity of the static

magnetic field could in some cases ruin the temperature measurements, as they are in the same magnitude scale.

4.1.2 Phantom

Phantoms are often used for testing the liability of a certain medical imaging method. In MRI a phantom is usually an object trying copy the magnetic properties of a living tissue. Phantoms can be used to optimize the MRI examination before the patient is scanned. The benefit of using a phantom over a test patient is obvious in the study of thermal behavior of a certain examination set up. If a MRI study needs to be done, although there is a potential risk for burn or thermal harm, the measuring assembly could be first tested with a phantom. Usual possible risk for a MRI related burn would occur when a patient have implants or additional measuring devices, such as pulse oximeter, need to be used.

There is also problems with phantoms. Phantoms generally emit higher signal than humans and have a different distribution of spatial frequencies. Phantoms usually have sharp edges which can result in major susceptibility effects and shimming problems. The filling materials may also have atypical relaxation times. When using phantoms, there is some practical consideration to remember: allow the phantom filling settle down and reach thermal equilibrium, avoid bubble formation and minimize mechanical vibration [11].

Figure 10 An example of one of the phantoms build for thermometry purposes. Phantom is plastic lunch box filled with agar gel.

First, a phantom made for the test of phase image visualization was made by placing 1dl oil and 1dl agar box to a 9dl water filled box. The idea was to have a phantom containing materials with different relaxation times. The main phantom used for thermometry measurements were plastic or glass boxes filled up with just agar

gel. This kind of phantom is pictured in Figure 10. Agar (or Agar Agar) is a powder made from seaweeds used such as gelatin to make jelly. Agar phantoms are suitable for general MRI studies [50], and PRF MR thermometry examinations [28]. I suggest getting agar powder from a pharmacy as it is likely purer than the food-grade agar purchased from grocery store. The Agar gel was cooked according to the Stanford Agar Phantom Recipe (UCSD,USA). With the exception that no contrast agent (nickel chloride) was used. Also Atamon (used for jellies) and ascorbic acid, was used as preservatives instead of sodium azide. Sea salt is used for mimicking the radio frequency load of a living tissue. Here's the used recipe:

833 dl	*Tap water*
25 g	*Agar Agar powder (Oriola, Finland)*
4 g	*Sea salt*
½ tsp	*Atamon*
½ tsp	*Ascorbic acid*

In some recipes (FBIRN), the agar gel was cooked in a microwave oven, but I used a stove and a steel pan for better control of the temperature. Ingredients were measured with an Accurat 6000 electronic postal scale (Wedo, Germany). Use warm tap water and add agar agar powder and salt stirring simultaneously. Cook it up stirring just until it boils. Turn the stove off and let it cool a bit. The atamon and ascorbic acid can now be added, they are not meant to be boiled. Pour the agar to phantom at ~60-70˚C and let it rest for 24 hours at room temperature. The boiled agar gel will solidify when it is cooled under 45˚C. Again the solid agar gel will melt somewhere around 80˚C. This recipe will make about 9dl of solid agar gel.

If some additional instrumentation is needed in the study, in this case a thermal sensor and a heating resistor, they must be inserted in the warm liquid agar prior to cooling process. Afterwards inserted objects will fracture the solid agar gel, leaving air cavities. Another tip is to make big enough phantoms: *e.g.* 3 dl agar phantom was too small for the MRI scanner to acquire signal from. Agar phantoms made with this recipe will be preserved about two months in a refrigerator. If stored in a refrigerator, be sure to bring the phantom fully back to the room temperature before making temperature measurements.

4.1.3 Conventional thermometry

Proton resonance frequency method for measuring temperatures with MRI scanner can tell the phase shift difference originating from the temperature change. The method cannot tell the absolute temperature, but the change of temperature. That is why the starting temperature before the temperature change need to be known. For *in vivo* studies the starting temperature is the body temperature which can even be measured prior the MRI scan with conventional methods. Usual the method for acquiring a local temperature value in MRI phantom examinations is to use an optical thermal sensor. An optical sensor does not contain metal which could lead to possible artifacts in the image. The huge disadvantage of an optical sensor is it's fragility versus price index. Optical probe is precise but very frail temperature measurement instrument. A metallic thermocouple method was used to measure the initial temperature at the phantom. The obvious benefits of thermocouples are theirs robustness, inexpensiveness and the ease of use. The thermocouple sensors are also easy to do-it-yourself, so one can define *e.g.* the length of the sensor. Thermocouple consists of two different types of metal which have a particular temperature dependent voltage between them. The voltage between the known two metals is directly proportional to the temperature. The relation of voltage and temperature is unique for two particular metal couples, and is called a Seebeck coefficient. When building thermocouples, it should be noticed that also the connector should be made from the same metal types that are used in the wires.

A T-type PVC coated thermocouple (Electronic Temperature Instruments Ltd, United Kingdom) shown in Figure 11 was used to measure initial temperature in the MRI studies. The T-type thermocouples used, included a non-magnetic copper and a constantan wires made from seven 0,2mm fibers which are suitable for temperature measurements in the -200˚C to 400˚C range. First the basic more common K-type thermocouples where tried to be used, but they were too ferromagnetic and were effected by the static field. K-type thermometers have over 90% nickel which is ferromagnetic and also makes huge artifacts to the MR images.

Figure 11 T-type thermocouple and Ambrobe TMD-56 thermometer used in the thermometry studies. The exposed wires at the tip of the thermocouple were finally coated with thin plastic sock. Notice that the wires and corresponding connectors are made from same metal.

The digital thermometer used was Amprobe's (Amprobe, USA) model TMD-56 with basic accuracy of 0,05%. The thermometer is battery operated and with data logging ability. The data logging ability made it possible to leave the thermometer inside the shielded MRI room, and read the temperature values afterwards. Thermometer was also shielded with a custom made copper coated box in order to minimize the possible electromagnetic harms. When choosing additional measuring instruments for MRI studies it is always good to consider the possible harmful electromagnetic effects. The room is shielded for a reason, and no conducting wires should be passed through the walls if not absolutely necessary. Battery operated electronics exclude the need for external power sources from outside the shielded room.

4.1.4 Heating methods

In order to use MR thermometry, first some heat change needs to be generated. MRI guided thermometry therapies are usually done with an ultrasound or a laser. In this case the heating of the phantom was done with a heat resistor. First the concept of PRF thermometry was tested by placing a pre heated phantom in the bore and observing the cooling of the phantom. Agar filled phantom was heated keeping it 15 minutes in 70-75˚C water bath. It should be noticed that agar has a melting point of ~80˚C depending of the agar concentration. Then the hot phantom was placed in the 32-channel head coil, and the cooling of the phantom was observed with the PRF thermometry method.

Second heating test was done by placing a pre heated glycerol-water hot pillow (Thermal Care, Finland) over a room temperature agar phantom. The pillow was placed in straight contact with the agar gel, and then the heat distribution was observed with a 32-channel head coil. In PRF thermometry it is easier to measure accurate temperature change if there is also some area where no temperature change occurs. Then the signal information from the area with constant temperature can be used for correcting the baseline drift of the static magnetic field of the scanner. That is why this kind of heated pillow test was used, after observing the temperature reduce of the whole pre heated phantom. A heated pillow allowed the observation of the heat change of a smaller region rather than the whole phantom.

The goal was to make a remote controlled heating device which could be used to heat the phantom in MRI environment. With remote controlled heating device it would be possible to change the temperature of the phantom without having to enter and leave the room, move the patient table, and add any material to the imaging area. First tests were done by heating different kinds of small resistors with a 6V, 7,2Ah (HQ,China) lead gel battery. The battery was used inside the feedthrough pipe, waveguide, of the shielded room. The highly ferromagnetic battery were inserted to the waveguide, for safety reasons, from the outside of the room. The wires were PVC insulated, twisted, tin coated copper pairs. Twisted wires cancel out the possible harmful electromagnetic induction. The heating was pleasantly rapid, but even the smallest 5mm long commercial available metal resistors placed in the agar gel produced huge artifacts in the acquired MR images.

The tin coated copper wires themselves did not yield artifacts in the images. The idea of the non-metallic resistor arose. Common non-metallic electric wire consists of carbon fibers, which gave the idea of the carbon based heat resistor. It has been reported that carbon fiber produces virtually no artefacts in MRI [48]. Carbon fiber heaters are used *e.g.* for heating Formula 1 racing car tires before the race. At first, different carbon fiber fabrics were tested for the heating, but the warm up was too slow and copper wire connecting was hard. Then carbon fiber pipes were tested as a heat resistor and the heating was rapid with small diameter pipes, and connection of the wires were easy to a solid object rather than a piece of fabric. The chosen carbon fiber pipe used had 6mm diameter with 1mm wall thickness. Length of the pipe was about 70mm and the wires were twisted and welded at the opposite ends. In order to get good wire connection and uniform heat distribution, the wires were twisted tightly around the pipe for the length of 15mm and weld together. If just couple loops would be used, only thing heating

would be the connection between the wire and the carbon pipe. The wire welded on the far end was guided through the pipe from the other end. The PVC coat of the wire was reported to sustain a temperature of 120˚C. The result was a 70mm long non-ferrous MRI suitable remote controlled heating device. The heating device was placed inside a heat durable glass lab tube (DuPont, USA) which was then filled with silylated modified polymer glue (Superfix, Sweden) with 100˚C heat durability in order to secure it in it's place and get even more balanced heat distribution. The idea was that the solid glue would conduct the produced heat much better to the surrounding glass pipe, than the pipe filled only with air. The heating device was immersed in the liquid phantom during the agar cooking process. The constructed non-ferrous MRI compatible glass tube heating probe is portrayed in Figure 12. The heating device was used between the PRF thermometry imaging sequences.

Figure 12 The tip of the heating device before it was filled with silicon glue and infused in to the agar phantom

4.2 Signal processing

4.2.1 Optimization of imaging parameters

A gradient echo sequence is used to produce the thermometric data in MR thermometry. To optimize the gradient echo for the thermometry study, the signal arising from the temperature-dependent phase shift must be emphasized. Now that the relaxation times of the target are known, it is time to optimize the signal parameters. The temperature dependent phase difference signal-to-noise ratio $SNR_{\Delta\phi}$ can be estimated as:

$$SNR_{\Delta\phi} = \frac{|\,\Delta\phi(\Delta T)\,|}{\sigma_{\Delta\phi}} \tag{22}$$

where $\Delta\phi(\Delta T)$ is the phase shift induced from the temperature change at the target tissue, and $\sigma_{\Delta\phi}$ is the standard deviation of the phase image without the temperature change. Phase difference SNR is directly dependent to the gradient echo image intensity, so the $\sigma_{\Delta\phi}$ needs to be minimized to get the perfect MR thermometry signal.

The gradient echo image intensity is dependent on the tissue parameters T_1, T_2^*, and imaging parameters TE (echo time), TR (repetition time), and FA (flip angle). The signal intensity of a phase image is proportional to the TE with equation:

$$SNR_{\Delta\phi} \triangleq TE \cdot e^{-TE/T_2^*} \tag{23}$$

Which indicates that the optimal temperature measurement sensitivity is acquired when:

$$TE = T_2^* \tag{24}$$

Maximun temperature sensitivity, with echo time of near T_2^*, have been examined and proven *in vivo e.g.* in muscle and kidney [24]. The used TE defines the shortest TR that can be used. The TR is determined on how many slices are used and how long TE is, and it should be as short as possible to speed up the measurement. When the TR is chosen, it can be used to determine the optimal flip angle by Ernst relation:

$$\theta_E = cos^{-1}(e^{-TR/T_1}) \tag{25}$$

where θ_E is the optimal angle, or the Ernst angle.

4.2.2 PRF Thermometry sequences

Generally any kind of gradient echo sequence can be used to produce temperature maps in PRF MR thermometry. This gives the method quite good temporal and spatial resolution. Gradient echoes are typically so fast that it is possible to take volumetric thermometry maps in adequate time. The magnetic resonance imaging examination is always a compromise of different desired attributes. One examination may need to emphasize the spatial resolution, while other investigations needs a larger volume with negligible resolution. The trade-off depends on

the diagnostic value which is to be created. Sequence characteristics may also be based on the coil used in the study.

In this thesis, the idea was to use a 32-channel head coil to produce volumetric thermal map of an object size of phantom which could be built with a common household utensils. Phantoms used, had a volume of about 1 liter, with maximum dimensions under 20cm. There are lots of values to change, and here are some of the most important for a PRF thermometry: Scanning sequence GR, Slice thickness 1,5mm, repetition time 3790ms, echo time 30ms, number of averages 1, no gap, 100% sampling, 34,37% phase field of view, bandwidth 260kHz, matrix 256x88, flip angle 81, field of view 134x390, transversal orientation, voxel size 1,5mm^3, GRAPPA (Generalized autocalibrating partially parallel acquisition) factor 6. A smaller phase field of view was used because of the shape of the phantom, in order to speed up the examination time. These parameters lead to an acquisition time 3min 28s.

Generally in MR thermometry guided thermotherapy a negligible resolution would be magnitude of 1˚C/1min/1cm^3. PRF thermometry can perform at resolutions of standard deviation less than 1˚C, below 1s, in 2mm^3 [2].

4.2.3 Phase unwrapping and mapping

Each voxel in the target will emit an echo that has its own frequency and phase characteristics. If during the read-out, a voxel emits an echo with slightly different frequency or phase than anticipated, its location appears in wrong place. Then intensity of the reconstructed signal will be misplaced which leads to image artifacts. Phase image of a target will represent the phase of an emitted echo originating usually from a multi channel coil. In Figure 13, on the left is an example of a phase image

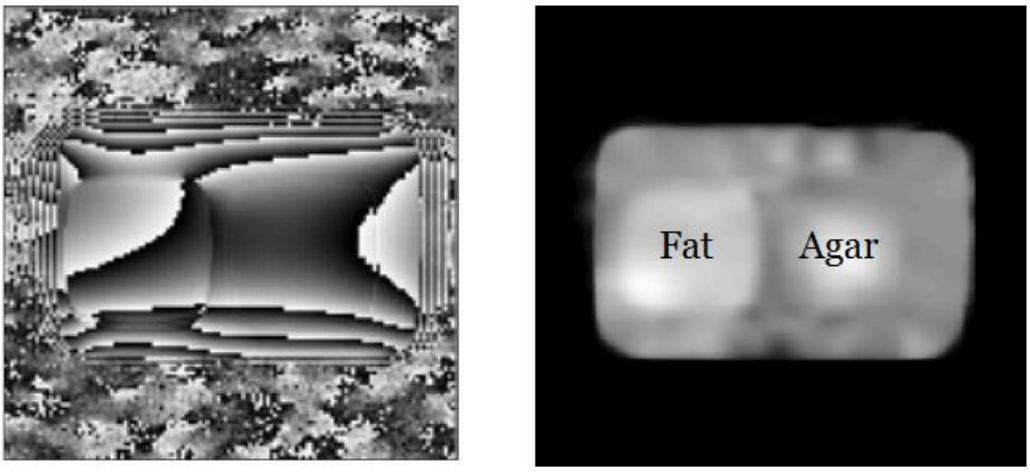

Figure 13 Transversal wrapped phase image of a phase phantom. Phantom has a fat and an agar component to guarantee uneven phase distribution. The image on the right is unwrapped field map image made with MATLAB's SPM8.

containing wrapped phase from a 32-channel head coil. In the Figure 14, on the right, is an unwrapped phase distribution of an echo from a lunch box phantom containing smaller fat, and agar boxes in a water bath. Phase wrapping appears at the border of a white and black stripe, on the left side image. These white and black should represent almost the same color, but the phase jumps 2π, from – π to + π or *vice versa*. To be able to compare the field maps of different images, we need first to unwrap these phase images. The right side of Figure 13, is the result from unwrapping the left side of the image. Unwrapped phase image contains no steep phase jumps, and can so be compared to other similar phase images.

In multi echo imaging, a slightly disturbed frequency leads to a continuous phase-development in consecutive echoes. Although, if a single echo imaging method is used over and over, one after the other, the errors in every echo manifests in same way. Relative errors between the echoes of multi echo imaging are in this way cut out. If two otherwise similar sequences are used with just different echo times, the speed of phase change can be observed. It means that a frequency map from phase difference can be calculated. Field map can be calculated from the frequency map with Larmor equation.

Unwrapped phase θ of the phase image can be noted as:

$$\theta_i = \phi_i + 2\pi n_i \quad n_i = 1,2,3 \ldots \tag{26}$$

where ϕ is the wrapped phase. First two dimensional phase unwrapping algorithms were introduced in 1988 by Goldstein *et al.* [41]. One of the phase unwrapping algorithms used in this thesis is called PRELUDE (Phase Region Ex-

panding Labelled for Unwrapping Discrete Estimates). The PRELUDE algorithm is part of the FSL (FMRIB Software Library) software written in C++ by members of the Analysis Group, FMRIB, Oxford, UK. This algorithm widely used in medical imaging for unwrapping the phase images, solves the problem by first dividing the whole volume in to N regions, which contains no phase wrapping. The number of these regions is much smaller than number of voxels, which provides noticeable increase in the calculation speed. Then a cost function sufficient for the job is one that penalizes phase difference along the interface of two unwrapped regions *A* and *B*:

$$C_{AB} = \sum_{j,k \in N(j)} (\theta_{Aj} - \theta_{Bk})^2$$

$$= \sum_{j,k \in N(j)} (\phi_{Aj} - \phi_{Bk} + 2\pi n_{AB})^2 \quad (27)$$

where $n_{AB} = n_A - n_B$ and n_i is the integer offset of the region in question. The sum is over two indices *j* and k, where *j* is the index of a voxel in *A* region, and k is the index of a voxel in *B* region. The total cost function that needs to be minimized over the whole volume is the sum of every one of these interfaces between region *A* and *B*. The solution can be determined with additional region merging algorithm described more detailed in FMRIB technical report [72]. FSL has also many other useful image processing features such as mask calculation tools *etc.* FSL is optimized to be used with Siemens MRI scanners.

Other software used to unwrap the phase images in this thesis is SPM8 toolbox written in MATLAB by Wellcome Trust Centre for Neuroimaging, UCL, UK. PRELUDE algorithm is also one of the unwrapping algorithms SPM uses. SPM can also use unwrapping algorithm specially developed to be used in image distortion correction in fMRI by Hutton *et al.* [73]. SPM is useful for removing the geometric deformations in EPI sequences, which is done with the aid of unwrapped phase image [73]. MATLAB was used in this thesis as a main signal processing tool other than just unwrapping the phase images. That is why SPM toolbox was also used in phase unwrapping. The results with SPM and FSL where not always the same for unwrapping. In some cases the FSL failed to unwrap the phase image with sharply wrapping corners, although FSL seemed to perform slightly faster than SPM.

Both FSL and SPM uses NIFTI image format, but the MRI scanner produces DICOM format images. MRIcron software by Chris Rorden has a drag and drop DI-

COM to NIFTI converter (dcm2niiGUI) which was used to convert images to the right format. Skyra scanner generates a DICOM image from every slice so that *e.g.* a sequence with 100 slices would produce 200 files, half magnitude and half phase images. DicomBrowser software written by Neuroinformatics Research Group, Washington University, was found helpful in examination of the DICOM images. A NIFTI image has either one .hdr (header) and a .img (disc image file), or just one .nii file. One NIFTI contains the whole entity of the slices, so the number of NIFTI's in gradient echo sequences is two: a magnitude, and a phase image file.

4.3 Measurements

4.3.1 T_1 and T_2^* relaxation time measurement

In many MRI examinations it is beneficial to know the relaxation characteristics of the target tissue. In MRI the nature of the magnetic relaxation lies on many factors such as the strength of the scanners magnetic field, the temperature and chemical composition of the tissue.

T_1 relaxation time can be measured with an inversion recovery method which is based on the initial 180 degree flip of the longitudinal relaxation of the net magnetization. Inversion recovery, pictured in Figure 14, starts with 180 degree flip of the net magnetization, then an inversion time (TI) is waited, and finally a spin echo sequence is applied. This way it is possible to dim certain parts of the target when the target's T_1 time is known. Inversion recovery can also be used to calculate the T_1 relaxation time, when the TI, that dims the target, is first discovered.

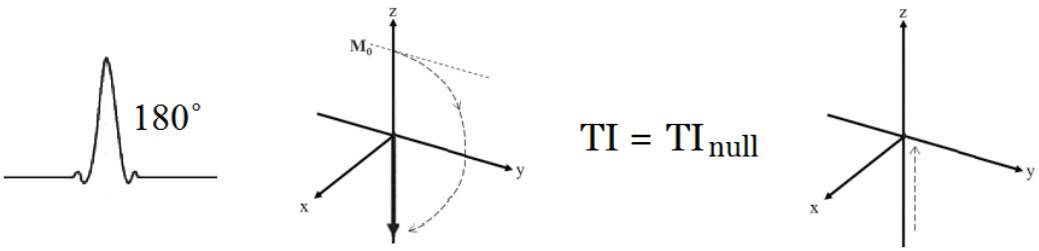

Figure 14 Inversion recovery pulse starts with a 180 degree pulse. Then an inversion time (TI) is waited, and a spin echo is applied. Spin echo cancels out the FID that arises from the lateral relaxation. Inversion time that minimizes the vertical part of the FID is called TI_{null} and is the time when the phantom appears the darkest.

Inversion recovery sequence with different TI times can be applied in order to find out the TI time that dims the image the most. The inversion time, that produces the darkest image, is called TI_{null}. Inversion recovery sequence is a spin-echo that starts with a 180° RF pulse, and then continues as a conventional spin-echo. In spin-echo sequence, the second 180° pulse after the initial 90° pulse cancels out the signal arising from lateral, or spin-lattice relaxation. Spin-spin relaxation time can then be estimated from the equation:

$$T_1 = \frac{TI_{null}}{ln2}, \tag{28}$$

where TI_{null} is the inversion time that minimizes the vertical part of the FID. Inversion recovery images could first be acquired *e.g.* with 500ms intervals, and later in smaller periods near the assumed TI_{null}. If some magnitude image recorded with longer time intervals appears even a little darker than others, the inversion time interval should be halved near that inversion time. For example if images with inversion times 500ms, 1000ms, and 1500ms are taken, and the image with TI = 1000ms appears the darkest, then next inversion times examined should be 750ms and 1250ms. This kind of iteration method is called bisection method. As the smallest possible interval for the inversion time the scanner allows is 10ms, one should be able to narrow down the results in less than ten iterations depending from the length of the initial TI step. The plan is to take inversion recovery images from the phantom with different inversion times, and seek for the darkest image with bisection method.

T_2^* relaxation time can be estimated with gradient echo pulse by observing the FID with different TE times. T_2^* is related to the echo times and the intensities of magnitude images according to equation:

$$T_2^* = \frac{TE_1 - TE_2}{ln\frac{I_{TE2}}{I_{TE1}}}, \tag{29}$$

where I_i is the intensity of the magnitude image. The idea is to take gradient echo images from the phantom, and compare the image intensities from the magnitude images. The study should be repeated multiple times, and use the mean value of the resulting T_2^*.

4.3.2 One slice PRF thermometry

In order to test the concept of PRF thermometry, some single slice gradient echo sequences will be taken from a phantom that is in changing temperature stage. The agar phantom is to be imaged with 32-channel head coil. The temperature change will be made with placing a hot object straight on the top of the unlidded agar gel phantom. It should be noticed that when starting a MRI examination, first a localizer sequence needs to be taken. Images from the localizer sequence are used to position the actual gradient echo sequences used in the PRF thermometry study. While placing the hot object on the agar, exiting the room, starting the localizer sequence, and waiting it to finish, a good two minutes has already gone before the start of the actual examination. During these two minutes, the agar phantom has already warmed up before taking the reference image, which should represent the starting temperature, as PRF is a relative temperature measuring method. This can be corrected in later thermometry studies including remote controlled heating device.

4.3.3 Volumetric PRF thermometry

The purpose of this thesis is to produce volumetric thermometry maps with proton resonance frequency shift method. In order to get accurate temperature measurement, the reference image should be taken before any temperature change occurs. This could be accomplished by the aid of remote controlled heating device. Like any MRI examination, the volumetric PRF study starts with a localizer sequence, and then the size and place of the target determines the parameters of the gradient echo sequences used to produce the volumetric thermal maps. After taking the localizer sequence, the physician has time to prepare the sequence queue, before starting the examination. It should be noticed, that if a mask image needs to be taken, it should be taken after the thermometry examinations, as it is usually a demanding spin echo sequence that can alter the homogeneity of the static magnetic field. If the mask image would be taken before the PRF sequences, an additional shimming of the static field should be used.

All the gradient echoes should be identical, so that the place and size from every produced image matches. This can be accomplished by setting the scanner to take multiple images with the same GRE sequence, and having the scanner to pause between sequences. These kinds of pauses are available because, in clinical MRI, they are used to *e.g.* administrate intravascular contrast agents. As the used heating device works with electricity, heating is to be done only while the scanner is on pause. The heating device heats from room temperature to about 70 °C, in two minutes. The gradient echo sequence used for temperature measurement study should not last for too long, and the voxel size should be as small as possible. Voxel size should also be isotropic so that the object would look the same from every angle. 2D sequential plane imaging technique is to be used as the use of 3D sequences leads to significantly longer acquisition time.

5 Results

5.1 Static magnetic field drift

The static magnetic field of the MRI scanner is known to drift in intensive use. Especially in the MR thermometry, it is important to make sure the magnetic field does not drift, or remove the error from a drift, because it may completely ruin the measurement as it is in the same magnitude. In this case, when measuring temperature dependence in the magnitude of 0,01ppm, the same PRF method could be used to demonstrate the existence of the base magnetic field drift. The PRF method was used to record the possible static magnetic field drift in the following manner:

1. shimming	PRF reference	wait without heating	PRF field drift measurement
2. shimming	PRF reference	heating	PRF temperature measurement

Where first the field drift was recorded and presented as it was a temperature change. Then the actual heating was done and the temperature measurement made. The used two measurements were identical, and scanners automatic shimming was used just before both to guarantee the same field conditions prior to measurements. This is a handy way of examining the static magnetic field drift, and it can also be used to correct the temperature measurement. Downside with this method is that it doubles the measurement time needed. Although, if there is no apparent static magnetic field drift, no drift induced temperature correction is needed.

The scanners ability to maintain the static magnetic field relates to for example the size of a target and measurement time. In some PRF tests lasting for longer than 15 minutes the drift started to show as a temperature change. In most of the cases the PRF measurements were shorter than 5 minutes, and therefore the drift did not produce any error to the temperature measurements. To demonstrate the existence of the main magnet baseline drift, some demanding operation *e.g.* a balanced SSFP sequence can be used to agitate the magnet [42].

5.2 T_1 and T_2^* relaxation time of the phantom

The T_1 time for the agar phantom was measured with the inversion recovery method and the results were:

$$T_1 = \frac{TI_{null}}{ln2} = \frac{1380ms \pm 5ms}{ln2} \sim 1991ms \pm 7ms\,, \tag{30}$$

where TI_{null} is the inversion recovery time in which the phantom emitted the least amount of signal. The inversion recovery time was changed in $10ms$ intervals and the TI_{null} was $1380ms$, as seen in Figure 15. The darkest image was determined from the lowest SNR. The longitudinal relaxation time for the agar phantom were therefore about $1991ms$.

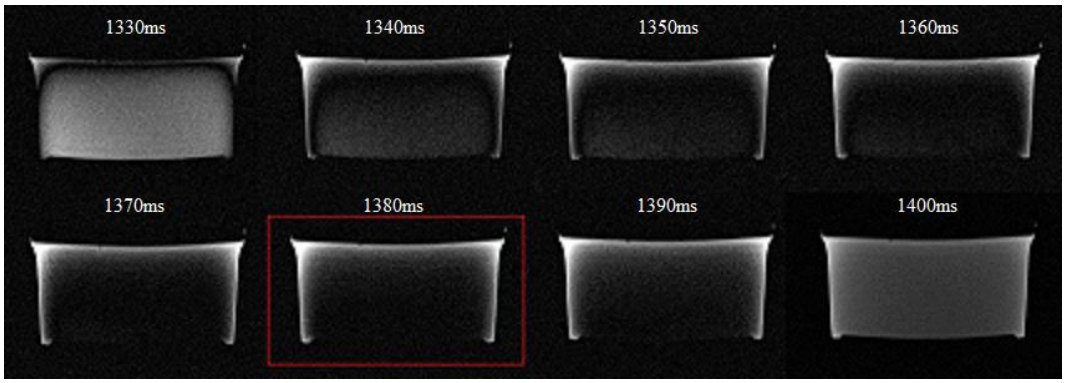

Figure 15 Agar phantom's T_1 relaxation time was measured with inversion recovery method, where inversion time TI = 1380ms represents the darkest highlighted image in the picture.

The lateral relaxation time T_2^* were estimated with two magnitude images with different echo times. A rectangle ROI inside the agar gel was chosen in the middle of the phantom. Two different images with $TE_1 = 5ms$ and $TE_2 = 10ms$ was acquired and the mean value of the chosen ROIs was compared. This test was repeated six times, with magnetic field shim after every two images. The ROIs where identical in every image. The six T_2^* results averaged at $T_2^* = 30{,}22ms$, with standard deviation, $SD = 0{,}1573ms$.

5.3 Echo time dependence of phase shift

The phase images of a phantom represent the spatial phase value map. The phase has values between -π and π. If the phase value goes over π, the scanner interprets the phase value starting again from -π. In phase image, this kind of skip is seen as stripe like wrapping of the phase. The two extreme values of the phase seem to be located next to each other. Of course this kind of wrapping makes it impossible to compare two slightly different phase shift images together.

Unwrapping algorithms often need a magnitude and a phase image to produce unwrapped field map. In agar phantom studies, according to the equation 24, optimal TE would be around 30ms, but as seen in Figure 16, the 30ms echo time wraps the phase image quite a lot. When comparing the unwrapping algorithm to phase images with different echo time, it was clear that the shorter the echo time the better the unwrapping worked. In Figure 17, it can be see how a phase image unwrapped with 30ms echo time has coarse edges, and an unwrapped phase image with 5ms echo time has much smoother edges. This happens because the magnitude image with 30ms echo time comes excessively bright and so has overly rugged edges.

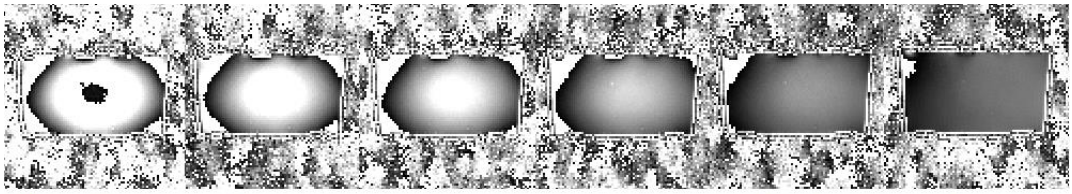

Figure 16 The agar phantom transversal phase images taken from the same location with different echo times (TE) to illustrate the wrapping of the phase with longer TE times.

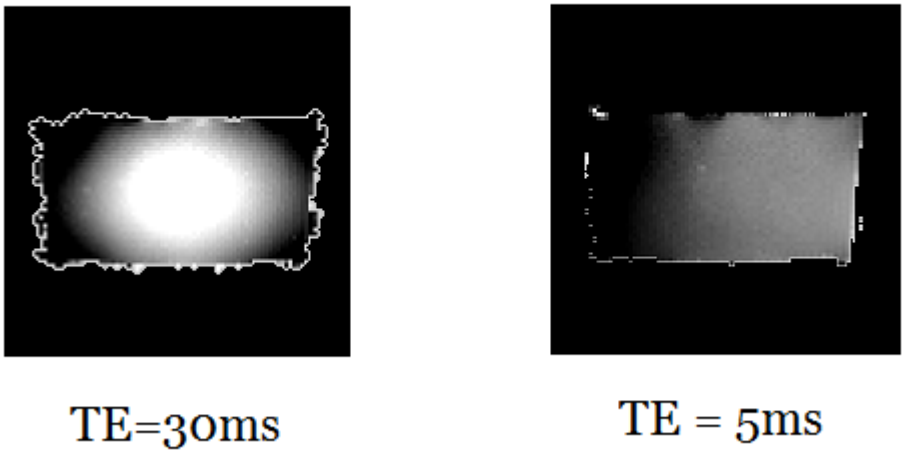

Figure 17 Two unwrapped phase images taken from same position from the agar phantom, with echo times 30ms and 5ms. The background of the images is masked black to emphasize the calculated phase at the borders of the phantom.

The temperature sensitivity for the agar phantom would be optimal with the 30ms echo time, but it takes at least 6 times as long to produce than a sequence with 5ms echo time, and it would need an additional mask to take out the erroneous rough edges.

5.4 PRF thermometry maps of the phantoms

5.4.1 First steps

The very first attempt to produce temperature maps from a phantom was done with agar-fat-water phantom preheated in water bath. The thought was to observe the temperature change as the phantom cools down to room temperature. By the time the PRF sequences was taken, the temperature change was too slow, and too much static magnetic field drift had been occurred, so that the formed thermal map did not make any sense. There was also problems with the phantom structure so a new one, containing only agar, was made for next studies. The first MR thermometry attempt taught that transversal slices had the least static magnetic field drift, as the drift usually appears in the Z-direction.

5.4.2 One slice heated pillow test

First successful thermal maps produced were from the measuring set up with just a pre-heated heating pillow on top of the room temperature agar gel. Prior the MRI examination, the agar phantom was placed in the room temperature for 24 hours. The room temperature was measured and added to the temperature value maps in the bottom of Figure 18. In Figure 18, the temperature induced phase change is demonstrated with wrapped black and white phase images reference, 3min, and 6min. The phase images change a little when the pre heated thermal pillow changes the temperature of the agar gel. The pillow was pre-heated to just below 80 degrees of Celsius, as that is roughly the melting point of the agar gel. The magnitude images stay the same. The colored images in Figure 18 have phase errors where the pillow is located, due to the fact that the heating pillow is made from a solution of glycerol and water, which is a very bad combination for a MRI phase image, as fat and water has totally different magnetic attributes. Usually in PRF thermometry studies, it is necessary to use fat suppression signal. Conventionally fat suppression is done with inversion recovery, but it can also be done with echo shift methods [14]. The agar part of the phantom contains hydrogen bonds in water, and so can be used to measure temperature with the PRF method. The background of the colored images serve as the room temperature, which was added to the relative temperature measurement between the time points. The image calculations where done with MATLAB according to equation 18. At this time, only one transversal slice was taken from the phantom, just to demonstrate the existence of the thermal change induced phase shift. The black dot in the center of the phantom was most likely an air bubble in the agar gel.

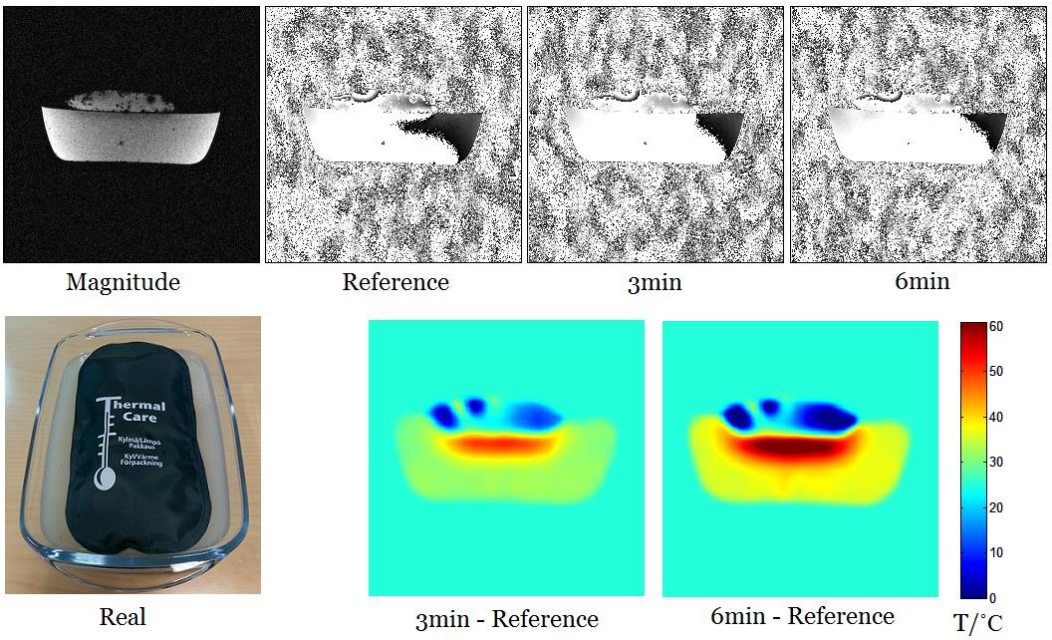

Figure 18 A magnitude image, and 3 phase images from different time points during the temperature measurement. The image labeled Real shows the pre-heated thermal pillow used. The two colored images at the bottom are produced from the phase images with image subtraction as they are labelled. It should be noticed that the agar in the reference image has already warmed up during the preparation of the scanner, before the actual phase images are acquired.

The colorbar in Figure 18, represents the calculated temperature change from phase shift with added room temperature. The reference image has already had some time to warm while preparing the scanner for the actual gradient echo imaging. That is why a remote controlled heating device should be used, in order to get accurate temperature values. Still, this examination proved the concept of PRF thermometry, as the phase changed during the heating of the agar gel. This change can even be seen straight from the phase images in Figure 18.

5.4.3 Volumetric and remote controlled measurements

The second PRF temperature measurement was supposed to be volumetric, and remote controlled. Also the temperature values should to be monitored straight from the agar, rather than just take an educated guess, that the phantom is at the room temperature. The heating device, the glass tube, and the two temperature measuring thermocouples were put through the plastic lid of the phantom, as seen in Figure 19. They were put in to the hot liquid agar before it was cooled down. One temperature sensor was positioned near the heating device to make sure there was some heating. Other thermocouple was stick to the other end of

the phantom to monitor the temperature of the phantom at place where no heating should occur. This way, if some heating would have been recorded with the sensor located far away from the heating device, the origin of the heating would have been unwanted heating due to the RF heating for example. But when only heating recorded with the thermocouples, was located near the heating device, there should not be seen any thermal change with PRF method, other than the real heating originating from the heating device. In other words, PRF method recorded the actual heating of the phantom, and not for example the possible static magnetic field drift. Although, in some cases when the thermometry sequence protocols where tested for roughly an hour, the phantom heated about one degree of Celsius from probably the RF heating. MRI scanner can estimate the SAR (Specific absorption rate) in these kind of cases, and stop the scan in order to prevent excessive heating of the patient, especially if the patient is small. In the case of phantoms, the inserted weight and height should be something an adult would have to prevent the scanner aborting the scan due to redundant SAR. In this study, the small phantom was bluffed to be a 75kg and 175cm patient. The gray part of the Figure 19 represents the agar part of the phantom, constructed with the FSL software. The hole of the heating device and two heat sensors can been as blank space.

Figure 19 The photograph of the phantom from above, and a binary mask created with FSL, which shows the part of the phantom containing agar. Pipe with grey wire is the heating device. Brown wires are the T-type thermocouples measuring the temperature.

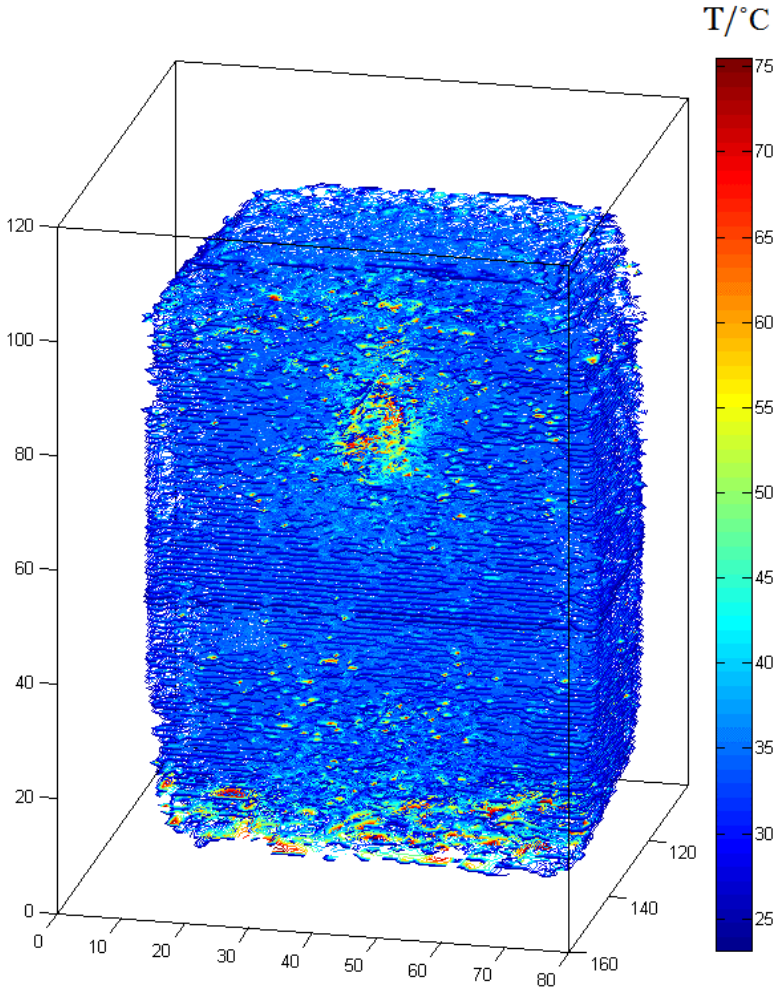

Figure 20 Volumetric thermal map made with proton resonance. The colors serve as degrees of Celsius calculated from phase maps. There can be seen errors at the edges of the thermal map, arising from the extreme steep air agar interface. Also there was some moisture on the bottom of the lid which gave phase artefact.

The actual volumetric thermal map of the agar phantom was built with MATLAB, and was based on the temperature induced PRF-coefficient of water (-0.01ppm). In Figure 20, the map was produced with a gradient echo sequence using 30ms TE (echo time), and the color bar temperature on the right, in Figure 20, is calculated with PRF-coefficient and TE time according to equation 18. The echo time length is inversely proportional to the temperature value. The used imaging frequency ($f_L = 2\pi\,\gamma B_0$) needed for the equation can be checked from the corresponding imaging files. The edges of the phantom produced artifacts containing the whole spectrum of the possible values that a DICOM image can have. The edge artefact values were neglected simply by taking a look some more reasonable temperature values between the room temperature and the agar gel melting point. This kind of filter method could still leave artefacts on the edge of the phantom. The edge artefacts could be removed with the aid of masks like the one on the right in Figure 19, and the one in Figure 21. Figure 21 is a cross section from the whole mask, showed from different angles to show the insides. The idea of a binary mask is that it contains zeros outside the agar interface, and ones inside the actual (agar) region of we are interested of. When the temperature data is multiplied with this kind of mask, outsides of the agar containing unwanted signal should not be seen. In Figure 21, no mask was used, other than the filter that passed through only the temperature values we were interested of.

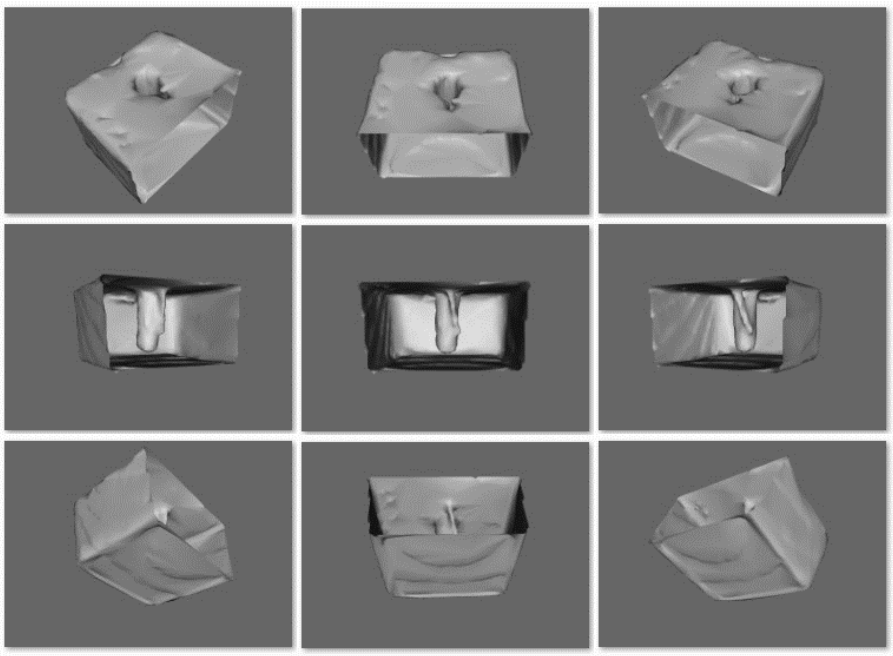

Figure 21 A cross-section of a binary mask that can be used to remove unnecessary values from the observed data. The interface is shown, where outside is zeros, and inside is ones. Mask is made with FSL (FMRIB, UK) software.

The axel values of Figure 20 and 22 shows slice numbers. The figures were made with 110 transversal 2D slices. The temperature values were mapped to the cross points of slices from X, Y, and Z plane with 1,5mm^3 voxel size. This way of contour slice plotting is an acceptable approach to take a look at value changes, as the PRF method records only the temperature change.

The third PRF temperature measurement was done with the same kind of gradient sequence, but with shorter echo time, repetition time, and lower flip angle. The echo time was now $5ms$. The idea was that the shorter echo time would get rid of the edge artefacts as demonstrated in Figure 17. Also in this case, a sequence with 5ms echo time can be made over 9,5 times faster than the one with $30ms$ echo time. That is because with lower echo time, repetition time could be also shorter. Lower echo time gives the PRF thermometry a reduced sensitivity as seen in Figure 9, but especially in the case of volumetric thermometry, the over nine times faster sequence and better unwrapping at the edges of the phase images, outweighs the smaller temperature induced phase shift sensitivity. The changed sequence parameters, were now: $TE = 5ms, TR =$ 230ms, FA=27°. The flip angle FA, was determined as Ernst angle (equation 27), and acquisition time was now 16 seconds per image.

In Figure 22, is a volumetric thermometry map of the same phantom set up, used to produce Figure 20, but it is presented another way around. Now the heating device is on the lower part of the phantom. The benefits of the lower echo time is obvious when observing the artefact on the edges of the agar gel in Figure 22. There is even no need to consider using mask to reduce the artefacts at the edges, which could be wise in the case of Figure 20. This examination with different sequence parameters were done on a different day to ensure that the phantom had time to return to the room temperature. The starting temperature were recorded and the MRI scanners fan was turned off in both cases.

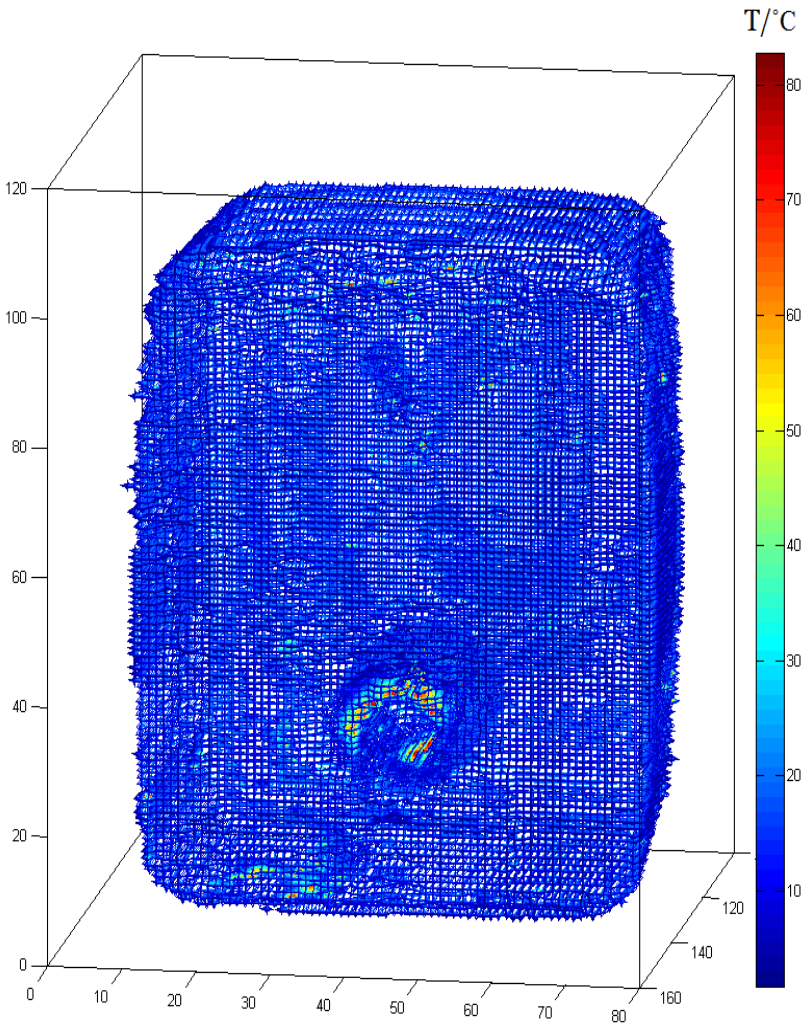

Figure 22 The volumetric PRF thermometry map from agar gel phantom, taken with 5ms echo time gradient echo sequence.

As the results for PRF thermometry measured from the sequence used in Figure 22 were satisfactory, it is appropriate to take a closer look. Figure 23 is a cross section of the same data used in Figure 22. As the volumetric contour lines plot the change in the data values, the unchanged temperature values inside the agar gel appears empty. This way it is possible to see inside a volumetric object and observe only the temperature change. Specifically, insides of the volume where no temperature induced phase shift exists, are shown empty, because they are at constant temperature.

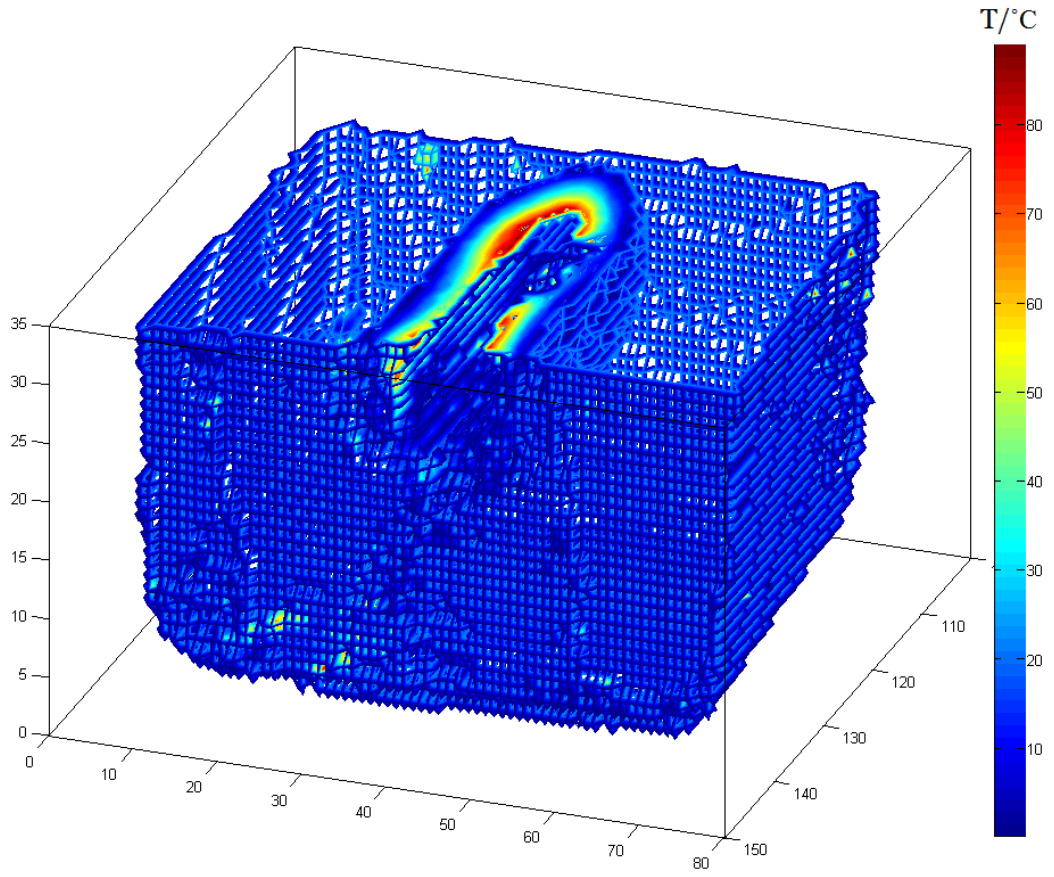

Figure 23 The cross-section of the agar phantom at the place of the heating device. The object appears empty, because only the temperature change is shown. The edges are seen because of the phase shift at agar outer interface.

5.4.4 Example applications

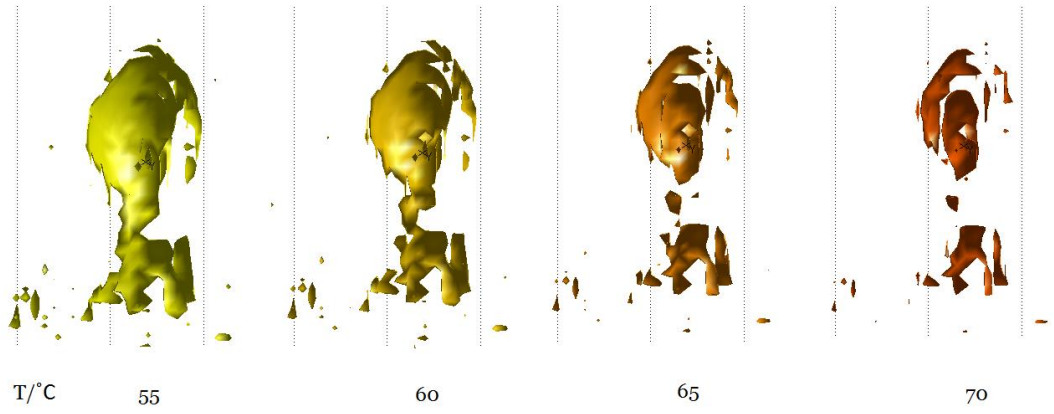

Figure 24 Particular volumetric temperature distributions at the tip of the heating device. Temperature volumes of 55, 60, 65, and 70˚C are shown as different colour. Light is added to emphasize the volumetric heat distribution.

In Figure 24, the temperature distribution in the agar gel, near the tip of the heating device, is represented with 5˚C increments. The figure is made with MATLAB as an isosurface. In some cases, temperature navigation is to be used to determine particular temperature thresholds. PRF MR-thermometry navigation can be used, when a tissue needs to be heated to a certain temperature in order to induce biological effect, such as a change in the protein structure [12]. Figure 24 shows volumetric distribution of certain temperatures with the aid of added light, to bring out the dimensions. The temperature is not symmetrically delivered to the agar gel, because the silicon glue inside the heating device did not evenly touch the inside surface of the glass pipe, which can be seen on the right side of the heating pipe in Figures 23 and 24. Also, the heating device is based on resistive heating, which makes the junctions between the wires and the carbon pipe hotter. The welded junctions can be seen in Figure 12. The errors in the Figure 24 are seen as dots and bubbles, and are most likely inflicted by impurities in the agar gel, because *e.g.* an air cavity in the agar gel induces a sharp change in the signal phase.

As the PRF MR thermometry is generally recognized to be accurate enough to be used as temperature change measuring purposes *in vivo*, here in Figure 25 is another sample of how the temperature could be monitored in three dimensions. The idea was to make temperature layers transparent, show multiple heat layers simultaneously, and add some light to show the volume.

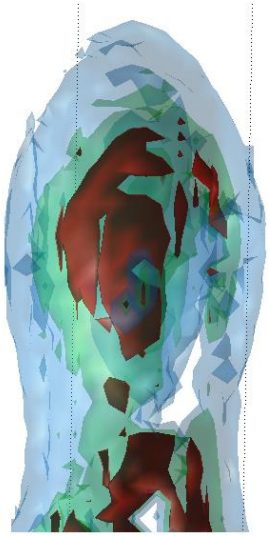

Figure 25 Different transparent temperature zones represented with rational colors. This is way the temperature guidance is more intuitive.

If the interest is on certain temperatures at the target tissue, it could be beneficial to remove other surrounding temperature values. In Figure 25, the noteworthy temperature volumes are displayed. The red color could represent certain threshold where temperature change is sufficient enough to produce desired biological reaction at the target. It could also represent the phase transition temperature for drug delivery phospholipid, above which local drug delivery occurs. The green color could serve as the safe zone, where the temperature shift does not induce irreversible change. The light blue color show the zone where only very little temperature change occurs, and could be used as a guiding aid. The temperature change could be done *e.g.* with the aid of laser, radio frequency, ultra sound, or infrared.

6 Discussion

The concept of interventional MRI focuses on *e.g*. MR-compatible instrumentation, minimal invasive thermal therapy, and even intraoperative MRI [13]. When using MRI as something other than just taking an anatomic image, we have to deal with creating new inventions. For instance, even the architecture of the scanner may have to be reconsidered. MRI is an imaging modality which full potential is not yet discovered. Nowadays there exists already different kinds of scanners for specific purposes. That is because MRI has so many functions. Whichever the scope of a MRI study is, the key to success lies in exceptional sequence design and signal processing. Every examination needs to be done as precise as possible, as fast as possible, and as safe as possible.

When considering PRF MR thermometry, it benefits from all the scientific innovations related to gradient echo imaging, because it could be done with virtually any gradient echo sequence that emphasize the phase information of a target tissue. Resent mentionable discoveries related to pulse design, increasing the MR thermometry performance, includes *e.g*. the MASTER sequence (multiple adjacent slice thermometry with excitation refocusing) [46], and referenceless PRF [27,30]. There is also numerous of methods to eliminate the possible baseline drift error, for example triggered sequences for *in vivo* studies [5, 19]. Finally, there is recent discoveries on the benefits of the adaptive filtering, feedback and interpolation techniques, and sequence design in real time MR thermometry [43, 53, 29, 26].

In real time thermometry, the signal processing time needs to be minimized. For example the referenceless PRF method does not need time consuming 2D unwrapping [27], which accelerates the study. However, the unwrapping problem can also be neglected by using real and imaginary images from the scanner, instead of magnitude and phase images. If the region of interest is very small, also a 2D complex estimation of the phase distribution can be used, to avoid the need for unwrapping [18]. Also many statistical techniques can be used, for example the baseline drift can be estimated from the apparent temperature change from nearby voxels located at sufficient distance from the heating device.

This thesis was a phantom study, so the challenges were related to non-clinical problems. When building agar phantoms, agar gel bubble formation could be decreased by reducing the surface tension of the media. For this problem, some solvent, such as ethanol could be the answer, as it removes surface tension. One of the not so obvious aspects related to the accuracy of the measurements in this study, is the MRI room temperature. It was discovered that, regardless the air condition, the room temperature was higher usually at the end of the day, because the scanner had been in use, lights on, and people inside the room. It has been reported that the main magnetic field of the scanner even follows the cycle of the air condition in the MRI room [42]. In an *in vivo* study, the subject has quite stable regulate body temperature, but *in vitro* studies the target temperature can be nearly anything. The target's temperature has to be acknowledged when optimizing imaging parameters, and when comparing the results on different studies with particular thermal conditions.

When measuring temperature with conducting wire near electromagnetic coils, there is couple factors to be noticed. Firstly, the wires should not be near the resonant frequency of the RF signal in the air. Secondly the wires should not be near the coils. And finally, the wires should of course be twisted to take out the change of electromagnetic induction. In this study, the temperature measurement with thermocouples failed one time, when the wire were too close the used 32-channel head coil. The wire of the heating device was pre twisted dual wire. The thermocouple wires were not twisted, but when there was two channels, and two wires, they could be twisted together.

PRF MR thermometry is such a sensitive measuring method, that the scanner's temperature change could induce measuring errors. To get the most accurate analysis, the measurement should also be done with one transmitting and receiving coil to guarantee the temperature unity.

Magnetic resonance imaging as a volumetric thermometry guiding method has numerous of applications. One of the possible applications is implant heating phantom test in MRI [31]. In order to test the possible heating of a conductive object in phantom, a rather demanding MRI sequence needs to be used. The RF pulse combo in spin-echo could lead to RF heating in conductive article in phantom or tissue. Some phantom RF heating test were executed by using an agar or a pork meat phantom with conductive copper objects. The tests were done with receiving 32-channel head coil, and with turbo spin echo sequences with high turbo factor to multiply the amount of RF pulses used. No heating was noticed, even with various different copper wires and loops, in different positions. The head coil is in the center of the main bore, which might be the reason why no

heating was recorded, as the RF heating usually happens near the transmitting coil, in this case, the main bore coil.

Other future applications for MR thermometry could be to measure temperature for diagnostic or therapeutic purposes from hard to get locations. For example bone marrow temperature is hard to measure conventionally and it carries diagnostic information related to *e.g.* stem cell activity. Also, the diagnosis that is a certain tumor benign or malignant could be based on the target's temperature. In innovative therapeutic purposes, a discussion have been on the topic that temperature change in the back of an eye could induce protein changes that could possibly lead to better eye sight. The temperature change monitoring in these kinds of hard to get places for therapeutic purposes could be achieved with MR thermometry. These kinds of new measurement events could need some innovative additional instrumentation such as a reference material near the bone marrow for spectroscopic temperature measuring purposes, or the use of specifically fabricated contrast agent. The use of contrast agents could make it possible to determine certain temperature threshold in blood vessels.

7 Conclusion

In this thesis, the basics of the nuclear magnetic resonance and magnetic resonance imaging were introduced. Also, the purpose and motivation for MR thermometry studies were explained. The efficiency and the challenges of different MR thermometry methods were discussed. And the superiority of the PRF MR thermometry beyond other methods was justified.

The goal of this thesis, was to produce volumetric thermometry data with MRI proton resonance method. It was argued that in order to avoid measuring errors, particularly the one arising from static magnetic field drift, the thermometry measurement should be done as fast as possible. The imaging sequence parameters were optimized according to the magnetic relaxation properties of the target phantom. It was shown, that the lower the echo time, the faster the acquisition time would be in gradient echo imaging. It was also discovered, that shorter echo time would lead to better unwrapping results, especially at the edges of a volumetric object.

The results of the examinations in this thesis was first two dimensional temperature maps, and further, volumetric thermometry data of a whole object.

To sum up, this thesis showed how to perform a simple thermometry study in magnetic environment and how to easily use the MRI scanner's images to generate three dimensional thermometry map of a phantom. PRF MR thermometry can use any gradient echo sequence, and therefore, most of the huge number of methods available improving gradient echo imaging are usable. MRI has recently made big improvements related to different type artefact removing and signal analyzing methods, from which PRF thermometry, among other, now benefits.

References

[1]
J. D. Poorter, C. D. Wagter, Y. D. Deene, C. Thomsen, F. Ståhlberg, and E. Achten, "Noninvasive MRI Thermometry with the Proton Resonance Frequency (PRF) Method: In Vivo Results in Human Muscle," *Magn. Reson. Med.*, vol. 33, no. 1, pp. 74–81, 1995.
[2]
B. Quesson, J. A. de Zwart, and C. T. W. Moonen, "Magnetic resonance temperature imaging for guidance of thermotherapy," *J. Magn. Reson. Imaging*, vol. 12, no. 4, pp. 525–533, 2000.
[3]
W. A. Grissom, A. B. Kerr, A. B. Holbrook, J. M. Pauly, and K. Butts-Pauly, "Maximum linear-phase spectral-spatial radiofrequency pulses for fat-suppressed proton resonance frequency–shift MR Thermometry," *Magn. Reson. Med.*, vol. 62, no. 5, pp. 1242–1250, 2009.
[4]
J. D. Poorter, "Noninvasive MRI thermometry with the proton resonance frequency method: Study of susceptibility effects," *Magn. Reson. Med.*, vol. 34, no. 3, pp. 359–367, 1995.
[5]
K. K. Vigen, B. L. Daniel, J. M. Pauly, and K. Butts, "Triggered, navigated, multi-baseline method for proton resonance frequency temperature mapping with respiratory motion," *Magn. Reson. Med.*, vol. 50, no. 5, pp. 1003–1010, 2003.
[6]
R. D. Peters and R. M. Henkelman, "Proton-resonance frequency shift MR thermometry is affected by changes in the electrical conductivity of tissue," *Magn. Reson. Med.*, vol. 43, no. 1, pp. 62–71, 2000.
[7]
Y. Ishihara, A. Calderon, H. Watanabe, K. Okamoto, Y. Suzuki, K. Kuroda, and Y. Suzuki, "A precise and fast temperature mapping using water proton chemical shift," *Magn. Reson. Med.*, vol. 34, no. 6, pp. 814–823, 1995.
[8]
N. McDannold, "Quantitative MRI-based temperature mapping based on the proton resonant frequency shift: Review of validation studies," *International Journal of Hyperthermia*, vol. 21, no. 6, pp. 533–546, Sep. 2005.
[9]
K. Kuroda, R. v. Mulkern, K. Oshio, L. p. Panych, T. Nakai, T. Moriya, S. Okuda, K. Hynynen, and F. a. Joles, "Temperature mapping using the water proton chemical shift: Self-referenced method with echo-planar spectroscopic imaging," *Magn. Reson. Med.*, vol. 43, no. 2, pp. 220–225, 2000.
[10]
K. Kuroda, "Non-invasive MR thermography using the water proton chemical shift," *International Journal of Hyperthermia*, vol. 21, no. 6, pp. 547–560, Sep. 2005.
[11]
D. W. McRobbie, E. A. Moore, M. J. Graves, and M. R. Prince, *MRI from Picture to Proton*. Cambridge: Cambridge University Press, 2006.
[12]
N. J. McDannold, R. L. King, F. A. Jolesz, and K. H. Hynynen, "Usefulness of MR Imaging-Derived Thermometry and Dosimetry in Determining the Threshold for Tissue Damage Induced by Thermal Surgery in Rabbits," *Radiology*, vol. 216, no. 2, pp. 517–523, Aug. 2000.
[13]
T. Schulz, S. Puccini, J.-P. Schneider, and T. Kahn, "Interventional and intraoperative MR: review and update of techniques and clinical experience," *Eur Radiol*, vol. 14, no. 12, pp. 2212–2227, Oct. 2004.

[14]
J. A. de Zwart, F. C. Vimeux, C. Delalande, P. Canioni, and C. T. W. Moonen, “Fast lipid-suppressed MR temperature mapping with echo-shifted gradient-echo imaging and spectral-spatial excitation,” *Magn. Reson. Med.*, vol. 42, no. 1, pp. 53–59, 1999.
[15]
V. Rieke and K. Butts Pauly, “MR thermometry,” *J. Magn. Reson. Imaging*, vol. 27, no. 2, pp. 376–390, 2008.
[16]
M. O. Köhler, C. Mougenot, B. Quesson, J. Enholm, B. L. Bail, C. Laurent, C. T. W. Moonen, and G. J. Ehnholm, “Volumetric HIFU ablation under 3D guidance of rapid MRI thermometry,” *Medical Physics*, vol. 36, no. 8, pp. 3521–3535, Aug. 2009.
[17]
V. Rieke, K. K. Vigen, G. Sommer, B. L. Daniel, J. M. Pauly, and K. Butts, “Reference-less PRF shift thermometry,” *Magn. Reson. Med.*, vol. 51, no. 6, pp. 1223–1231, 2004.
[18]
K. Kuroda, D. Kokuryo, E. Kumamoto, K. Suzuki, Y. Matsuoka, and B. Keserci, “Optimization of self-reference thermometry using complex field estimation,” *Magn. Reson. Med.*, vol. 56, no. 4, pp. 835–843, 2006.
[19]
A. V. Shmatukha and C. J. G. Bakker, “Correction of proton resonance frequency shift temperature maps for magnetic field disturbances caused by breathing,” *Phys. Med. Biol.*, vol. 51, no. 18, p. 4689, Sep. 2006.
[20]
W. Wlodarczyk, R. Boroschewski, M. Hentschel, P. Wust, G. Mönich, and R. Felix, “Three-dimensional monitoring of small temperature changes for therapeutic hyperthermia using MR,” *J. Magn. Reson. Imaging*, vol. 8, no. 1, pp. 165–174, 1998.
[21]
W. Wlodarczyk, M. Hentschel, P. Wust, R. Noeske, N. Hosten, H. Rinneberg, and R. Felix, “Comparison of four magnetic resonance methods for mapping small temperature changes,” *Phys. Med. Biol.*, vol. 44, no. 2, p. 607, Feb. 1999.
[22]
D. Germain, E. Vahala, G. j. Ehnholm, T. Vaara, M. Ylihautala, M. Savart, A. Laurent, J. Tanttu, and H. Saint-Jalmes, “MR temperature measurement in liver tissue at 0.23 T with a steady-state free precession sequence,” *Magn. Reson. Med.*, vol. 47, no. 5, pp. 940–947, 2002.
[23]
N. McDannold, K. Hynynen, and F. Jolesz, “MRI monitoring of the thermal ablation of tissue: Effects of long exposure times,” *J. Magn. Reson. Imaging*, vol. 13, no. 3, pp. 421–427, 2001.
[24]
A. H. Chung, K. Hynynen, V. Colucci, K. Oshio, H. E. Cline, and F. A. Jolesz, “Optimization of spoiled gradient-echo phase imaging for in vivo localization of a focused ultrasound beam,” *Magn. Reson. Med.*, vol. 36, no. 5, pp. 745–752, Nov. 1996.
[25]
D. Moratal, A. Vallés-Luch, L. Martí-Bonmatí, and M. Brummer, “k-Space tutorial: an MRI educational tool for a better understanding of k-space,” *Biomed Imaging Interv J*, vol. 4, no. 1, Jan. 2008.
[26]
A. B. Holbrook, J. M. Santos, E. Kaye, V. Rieke, and K. B. Pauly, “Real Time MR Thermometry for Monitoring HIFU Ablations of the Liver,” *Magn Reson Med*, vol. 63, no. 2, pp. 365–373, Feb. 2010.

[27]
C. Zou, H. Shen, M. He, C. Tie, Y.-C. Chung, and X. Liu, "A fast referenceless PRFS-based MR thermometry by phase finite difference," *Phys. Med. Biol.*, vol. 58, no. 16, p. 5735, Aug. 2013.
[28]
J. Olsrud, R. Wirestam, S. Brockstedt, A. M. K. Nilsson, K.-G. Tranberg, F. Ståhlberg, and B. R. R. Persson, "MRI thermometry in phantoms by use of the proton resonance frequency shift method: application to interstitial laser thermotherapy," *Phys. Med. Biol.*, vol. 43, no. 9, p. 2597, Sep. 1998.
[29]
L. Agnello, C. Militello, C. Gagliardo, and S. Vitabile, "Referenceless thermometry using radial basis function interpolation," in *2014 World Symposium on Computer Applications Research (WSCAR)*, 2014, pp. 1–6.
[30]
W. Grissom, K. B. Pauly, M. Lustig, V. Rieke, J. Pauly, and N. McDannold, "Regularized referenceless temperature estimation in PRF-shift MR thermometry," in *IEEE International Symposium on Biomedical Imaging: From Nano to Macro, 2009. ISBI '09*, 2009, pp. 1235–1238.
[31]
E. M. Shapiro, A. Borthakur, M. J. Shapiro, R. Reddy, and J. S. Leigh, "Fast MRI of RF heating via phase difference mapping," *Magn. Reson. Med.*, vol. 47, no. 3, pp. 492–498, Mar. 2002.
[32]
H. E. Cline, K. Hynynen, E. Schneider, C. J. Hardy, S. E. Maier, R. D. Watkins, and F. A. Jolesz, "Simultaneous magnetic resonance phase and magnitude temperature maps in muscle," *Magn. Reson. Med.*, vol. 35, no. 3, pp. 309–315, Mar. 1996.
[33]
J. C. Hindman, "Proton Resonance Shift of Water in the Gas and Liquid States," *The Journal of Chemical Physics*, vol. 44, no. 12, pp. 4582–4592, Jun. 1966.
[34]
M. C. Bennett, D. B. Wiant, J. A. Gersh, W. Dolesh, X. Ding, R. C. M. Best, and J. D. Bourland, "Mechanisms and prevention of thermal injury from gamma radiosurgery headframes during 3T MR imaging," *Journal of Applied Clinical Medical Physics*, vol. 13, no. 4, Jul. 2012.
[35]
M. F. Dempsey, B. Condon, and D. M. Hadley, "Investigation of the factors responsible for burns during MRI," *J. Magn. Reson. Imaging*, vol. 13, no. 4, pp. 627–631, Apr. 2001.
[36]
M. F. Dempsey and B. Condon, "Thermal Injuries Associated with MRI," *Clinical Radiology*, vol. 56, no. 6, pp. 457–465, Jun. 2001.
[37]
H. Bassen, W. Kainz, G. Mendoza, and T. Kellom, "MRI-induced heating of selected thin wire metallic implants – laboratory and computational studies – findings and new questions raised," *Minim Invasive Ther Allied Technol*, vol. 15, no. 2, pp. 76–84, Jan. 2006.
[38]
T. O. Woods, "Standards for medical devices in MRI: Present and future," *J. Magn. Reson. Imaging*, vol. 26, no. 5, pp. 1186–1189, Nov. 2007.
[39]
C. J. Yeung, R. C. Susil, and E. Atalar, "RF safety of wires in interventional MRI: Using a safety index," *Magn. Reson. Med.*, vol. 47, no. 1, pp. 187–193, Jan. 2002.
[40]
S. Achenbach, W. Moshage, B. Diem, T. Bieberlea, V. Schibgilla, and K. Bachmann, "Effects of magnetic resonance imaging on cardiac pacemakers and electrodes," *American Heart Journal*, vol. 134, no. 3, pp. 467–473, Sep. 1997.

[41]
R. M. Goldstein, H. A. Zebker, and C. L. Werner, “Satellite radar interferometry: Two-dimensional phase unwrapping,” *Radio Sci.*, vol. 23, no. 4, pp. 713–720, Jul. 1988.
[42]
A. M. El-Sharkawy, M. Schär, P. A. Bottomley, and E. Atalar, “Monitoring and correcting spatio-temporal variations of the MR scanner’s static magnetic field,” *Magn Reson Mater Phy*, vol. 19, no. 5, pp. 223–236, Oct. 2006.
[43]
S. Roujol, B. D. de Senneville, S. Hey, C. Moonen, and M. Ries, “Robust Adaptive Extended Kalman Filtering for Real Time MR-Thermometry Guided HIFU Interventions,” *IEEE Transactions on Medical Imaging*, vol. 31, no. 3, pp. 533–542, Mar. 2012.
[44]
R. Salomir, M. Viallon, A. Kickhefel, J. Roland, D. R. Morel, L. Petrusca, V. Auboiroux, T. Goget, S. Terraz, C. D. Becker, and P. Gross, “Reference-Free PRFS MR-Thermometry Using Near-Harmonic 2-D Reconstruction of the Background Phase,” *IEEE Transactions on Medical Imaging*, vol. 31, no. 2, pp. 287–301, Feb. 2012.
[45]
V. Rieke, A. M. Kinsey, A. B. Ross, W. H. Nau, C. J. Diederich, G. Sommer, and K. B. Pauly, “Referenceless MR Thermometry for Monitoring Thermal Ablation in the Prostate,” *IEEE Transactions on Medical Imaging*, vol. 26, no. 6, pp. 813–821, Jun. 2007.
[46]
M. Marx, J. Plata, and K. B. Pauly, “Toward Volumetric MR Thermometry With the MASTER Sequence,” *IEEE Transactions on Medical Imaging*, vol. 34, no. 1, pp. 148–155, Jan. 2015.
[47]
J. A. de Zwart, F. C. Vimeux, J. Palussière, R. Salomir, B. Quesson, C. Delalande, and C. T. W. Moonen, “On-line correction and visualization of motion during MRI-controlled hyperthermia,” *Magn. Reson. Med.*, vol. 45, no. 1, pp. 128–137, Jan. 2001.
[48]
J. R. Reichenbach, S. Wurdinger, S. O. R. Pfleiderer, and W. A. Kaiser, “Comparison of artifacts produced from carbon fiber and titanium alloy needles at 1.5 T MR imaging,” *J. Magn. Reson. Imaging*, vol. 11, no. 1, pp. 69–74, Jan. 2000.
[49]
S. J. Matzat, E. J. McWalter, F. Kogan, W. Chen, and G. E. Gold, “T2 Relaxation time quantitation differs between pulse sequences in articular cartilage,” *J. Magn. Reson. Imaging*, p. n/a–n/a, Sep. 2014.
[50]
M. D. Mitchell, H. L. Kundel, L. Axel, and P. M. Joseph, “Agarose as a tissue equivalent phantom material for NMR imaging,” *Magnetic Resonance Imaging*, vol. 4, no. 3, pp. 263–266, 1986.
[51]
P. Tofts, *Quantitative MRI of the Brain: Measuring Changes Caused by Disease*. John Wiley & Sons, 2005.
[52]
S. Kanayamay, S. Kuhara, and K. Satoh, “In vivo rapid magnetic field measurement and shimming using single scan differential phase mapping,” *Magn. Reson. Med.*, vol. 36, no. 4, pp. 637–642, Oct. 1996.
[53]
J. K. Enholm, M. O. Kohler, B. Quesson, C. Mougenot, C. T. W. Moonen, and S. D. Sokka, “Improved Volumetric MR-HIFU Ablation by Robust Binary Feedback Control,” *IEEE Transactions on Biomedical Engineering*, vol. 57, no. 1, pp. 103–113, Jan. 2010.

[54]
C. Mougenot, B. Quesson, B. D. de Senneville, P. L. de Oliveira, S. Sprinkhuizen, J. Palussière, N. Grenier, and C. T. W. Moonen, "Three-dimensional spatial and temporal temperature control with MR thermometry-guided focused ultrasound (MRgHIFU)," *Magn. Reson. Med.*, vol. 61, no. 3, pp. 603–614, Mar. 2009.
[55]
"Real-Time Control of Focused Ultrasound Heating Based on Rap... : Investigative Radiology," *LWW*. [Online]. Available: http://journals.lww.com/investigativeradiology/Fulltext/1999/03000/Real_Time_Control_of_Focused_Ultrasound_Heating.6.aspx. [Accessed: 09-Apr-2015].
[56]
B. Quesson, C. Laurent, G. Maclair, B. D. de Senneville, C. Mougenot, M. Ries, T. Carteret, A. Rullier, and C. T. W. Moonen, "Real-time volumetric MRI thermometry of focused ultrasound ablation in vivo: a feasibility study in pig liver and kidney," *NMR Biomed.*, vol. 24, no. 2, pp. 145–153, Feb. 2011.
[57]
C. Mougenot, R. Salomir, J. Palussière, N. Grenier, and C. T. W. Moonen, "Automatic spatial and temporal temperature control for MR-guided focused ultrasound using fast 3D MR thermometry and multispiral trajectory of the focal point," *Magn. Reson. Med.*, vol. 52, no. 5, pp. 1005–1015, Nov. 2004.
[58]
R. T. D. Peters, R. S. Hinks, and R. M. Henkelman, "Ex vivo tissue-type independence in proton-resonance frequency shift MR thermometry," *Magn. Reson. Med.*, vol. 40, no. 3, pp. 454–459, Sep. 1998.
[59]
O. Dietrich, J. G. Raya, S. B. Reeder, M. F. Reiser, and S. O. Schoenberg, "Measurement of signal-to-noise ratios in MR images: Influence of multichannel coils, parallel imaging, and reconstruction filters," *J. Magn. Reson. Imaging*, vol. 26, no. 2, pp. 375–385, Aug. 2007.
[60]
M. Aşkin and A. Yilmaz, "The Calculation of Correlation Time (τ) for T 1 Spin–Lattice and T 2 Spin–Spin Relaxation Times in Agar Solutions," *Spectroscopy Letters*, vol. 37, no. 2, pp. 217–224, Jan. 2004.
[61]
R. N. Muller, L. Vander Elst, and S. Laurent, "Spin Transition Molecular Materials: Intelligent Contrast Agents for Magnetic Resonance Imaging," *J. Am. Chem. Soc.*, vol. 125, no. 27, pp. 8405–8407, Jul. 2003.
[62]
F. Settecase, M. S. Sussman, and T. P. L. Roberts, "A new temperature-sensitive contrast mechanism for MRI: Curie temperature transition-based imaging," *Contrast Media Mol Imaging*, vol. 2, no. 1, pp. 50–54, Jan. 2007.
[63]
M. Klarhöfer, B. Dilharreguy, P. van Gelderen, and C. T. W. Moonen, "A PRESTO-SENSE sequence with alternating partial-Fourier encoding for rapid susceptibility-weighted 3D MRI time series," *Magn. Reson. Med.*, vol. 50, no. 4, pp. 830–838, Oct. 2003.
[64]
G. B. Chavhan, P. S. Babyn, B. Thomas, M. M. Shroff, and E. M. Haacke, "Principles, Techniques, and Applications of T2*-based MR Imaging and Its Special Applications," *Radiographics*, vol. 29, no. 5, pp. 1433–1449, Sep. 2009.
[65]
D. L. Parker, V. Smith, P. Sheldon, L. E. Crooks, and L. Fussell, "Temperature distribution measurements in two-dimensional NMR imaging," *Medical Physics*, vol. 10, no. 3, pp. 321–325, May 1983.

[66]
D. Le Bihan, J. Delannoy, and R. L. Levin, “Temperature mapping with MR imaging of molecular diffusion: application to hyperthermia.,” *Radiology*, vol. 171, no. 3, pp. 853–857, Jun. 1989.
[67]
E. O. Stejskal and J. E. Tanner, “Spin Diffusion Measurements: Spin Echoes in the Presence of a Time-Dependent Field Gradient,” *The Journal of Chemical Physics*, vol. 42, no. 1, pp. 288–292, Jan. 1965.
[68]
R. T. D. Peters, R. S. Hinks, and R. M. Henkelman, “Ex vivo tissue-type independence in proton-resonance frequency shift MR thermometry,” *Magn. Reson. Med.*, vol. 40, no. 3, pp. 454–459, Sep. 1998.
[69]
E. Krestel, “Imaging Systems for Medical Diagnosis: Fundamentals and Technical Solutions - X-Ray Diagnostics- Computed Tomography - Nuclear Medical Diagnostics - Magnetic Resonance Imaging - Ultrasound Technology,” *Imaging Systems for Medical Diagnosis: Fundamentals and Technical Solutions - X-Ray Diagnostics- Computed Tomography - Nuclear Medical Diagnostics - Magnetic Resonance Imaging - Ultrasound Technology, by Erich Krestel (Editor), pp. 627. ISBN 3-8009-1564-2. Wiley-VCH , October 1990.*, vol. -1, Oct. 1990.
[70]
W. R. Nitz, A. Oppelt, W. Renz, C. Manke, M. Lenhart, and J. Link, “On the heating of linear conductive structures as guide wires and catheters in interventional MRI,” *J. Magn. Reson. Imaging*, vol. 13, no. 1, pp. 105–114, Jan. 2001.
[71]
J. L. R. Andersson, C. Hutton, J. Ashburner, R. Turner, and K. Friston, “Modeling Geometric Deformations in EPI Time Series,” *NeuroImage*, vol. 13, no. 5, pp. 903–919, May 2001.
[72]
M. Jenkinson, “Fast, automated, N-dimensional phase-unwrapping algorithm,” *Magn. Reson. Med.*, vol. 49, no. 1, pp. 193–197, Jan. 2003.
[73]
C. Hutton, A. Bork, O. Josephs, R. Deichmann, J. Ashburner, and R. Turner, “Image Distortion Correction in fMRI: A Quantitative Evaluation,” *NeuroImage*, vol. 16, no. 1, pp. 217–240, May 2002.